UNITED NATIONS UNIVERSITY
UNU-GTP
Geothermal Training Programme

Orkustofnun, Grensásvegur 9,
IS-108 Reykjavík, Iceland

Reports 2018
Number 13

1D JOINT INVERSION OF MT AND TEM DATA FROM NGOZI GEOTHERMAL PROSPECT, SW-TANZANIA – AN INTEGRATED INTERPRETATION OF GEOSCIENTIFIC RESULTS

Makoye M. Didas
Tanzania Geothermal Development Company, Ltd. – TGDC
P.O. Box 14801
Dar es Salaam
TANZANIA
geodidas@ymail.com, makoye.didas@tanesco.co.tz

ABSTRACT

Ngozi geothermal prospect is the flagship prospect of TGDC, located in the Mbeya region in the southwestern part of Tanzania. The prospect is within the southern part of the East Africa rift triple junction of Rukwa, Usangu and Karonga basins, which are located where the eastern and western branches of the East African Rift System converge and form an important volcanic zone, the Rungwe volcanic province. This report summarizes the integrated findings of resistivity models based on 1D joint inversion of TEM – MT sounding data and the previous geological and structural work of the area together with geochemical results.

Based on the integrated findings from this study three drilling sites are proposed to hit the reservoir, which is assessed to be 4 km wide and 7 km long. The low resistivity within the fault zone at a depth between 4 and 5 km below ground level (b.g.l.) south of Ngozi Caldera Lake is an evidence of the existence of the localized, relatively young, shallow plutonic bodies which may constitute a suitable heat source for the geothermal system. The eastern and western limits of extension of the reservoir correspond to the fault zones observed in the MT cross-sections south and north of Ngozi Caldera Lake. The eastern limit of the geothermal reservoir also corresponds quite well with the fault mapped during the surface geological survey. It has been observed that the shear zones, including most of the lineaments and inferred faults previously mapped in the area, cause displacement of the conductive anomalies in MT data.

Based on these findings, the geothermal conceptual model has been revised and a first priority zone of 28 km^2 was defined which has the maximum probability of hosting a geothermal system of 232°C reservoir temperature. The resource capacity of 49.4 MWe with a P90 probability has been evaluated through a volumetric assessment using Monte Carlo approach.

1. INTRODUCTION

Geophysics, particularly electrical resistivity methods, Magnetotellurics (MT) and Transient Electromagnetics (TEM) have over the past few decades been the most powerful geophysical tools in

surface exploration of geothermal systems. The Magnetotelluric (MT) method is a technique for imaging the electrical conductivity structure of the earth, from the near-surface down to a few tens of km (Chave et al., 2012). With the prevailing technology and discoveries, geothermal reservoirs located at a depth between 1 and 4 km can be economically exploited. With geophysical methods, the physical properties of the earth's crust are examined, but a common problem is that the resolution decreases with increasing depth. Complex geological environments with 3D resistivity behaviour have often been interpreted using simple 1D models. The 1D interpretation, where it is assumed that the resistivity only varies with depth, has been successfully used for decades (Ranganayaki, 1984; Ingham and Hutton, 1982; Park and Livelybrook, 1989; Chave et al., 2012).

When investigating geothermal systems, the resistivity anomalies found in MT surveys can be correlated with the overall permeability distribution of the reservoir. Rocks hosting geothermal fluids are usually characterised by relatively high resistivities overlaid by an impermeable smectite-clay rich layer with anomalously low resistivity. The heat source (i.e. shallow lying hot intrusive rock or a shallow magma chamber) leaks heat by conduction into the overlying reservoir and is characterized by anomalous low resistivity. The conductive anomaly in the clay cap is attributed to high cation exchange capacity of smectite clay minerals (Ussher et al., 2000). However, the smectite clays present in the cap rock prevents the formation of permeable open space at the top and margin of the reservoir, even where intersected by fractures (Cumming and Mackie, 2010). This clue of understanding the geometry of the conductive clay alteration is important to geothermal well targeting (Davatzes and Hickman, 2009). Therefore, the role of geophysics is to hunt the anomalies related to the geothermal system in the area.

Geophysical methods are not standalone methods. In order to constrain the geothermal system in the area, geophysical results should be integrated with geological, structural and geochemical results. These techniques help to reduce uncertainties and are very important components for the construction of the integrated geothermal conceptual models of the area.

This report describes data processing and interpretation of the 1D jointly inverted TEM and MT data from Ngozi geothermal prospect which is located at the southern triple junction within the East African rift system in the Rungwe volcanic province in SW-Tanzania. The report updates resistivity information previously published by Alexander et al. (2016). Also, it integrates results from geochemical studies and geological structures mapped in the area during a surface studies campaign in 2015 and 2016 (Alexander et al., 2016) and proposes three well drilling targets. Moreover, based on the integrated results, the resource is assessed using the Monte Carlo volumetric assessment.

2. GEOLOGICAL AND GEOTHERMAL CONDITIONS IN TANZANIA AND NGOZI AREA

2.1 Geological and regional tectonic setting of Tanzania

The African continent is gradually splitting apart along the East African Rift valley, a 3,000 km long series of deep basins and flanking mountain ranges (Figure 1). The East African Rift System (EARS) lies from the Afar region in SE-Eritrea and N-Ethiopia (Figure 1) forming the Afar triple junction. The rift stretches all the way south through Ethiopia, Kenya and N-Tanzania where it splits into two branches, the Eastern and the Western Rift. The two branches extend further south. In Tanzania, the two branches of the EARS converge at Mbeya area forming a triple junction within the Rungwe volcanic province (Delvaux and Hanon, 1993) before extending further south to Malawi and Zambia where it terminates. The EARS, being a continental-continental spreading plate boundary, is a potential area for geothermal resources in East Africa. Here, the continent is stretched, thinned and heated to the point of breaking. Hot, partially melted rocks rising up from the upper mantle are either erupting at the earth's surface or cooling within the crust. This is an important phenomenon which provides elevated heat sources for the geothermal systems. So far, Kenya is the only country in the Rift system that has taken use of the geothermal resource with over 600 MWe produced in Olkaria field. No potential geothermal

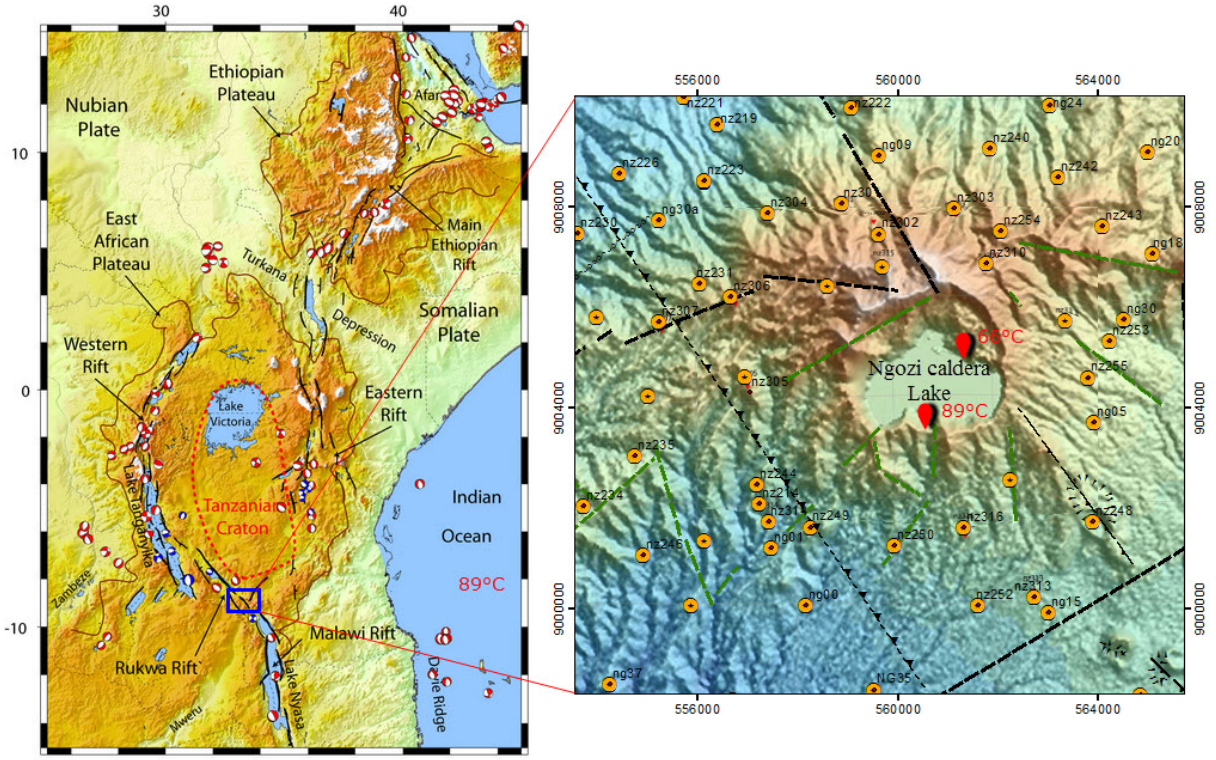

FIGURE 1: The East African Rift System: the red and white filled circles indicate the focal mechanisms for earthquakes in the area (Calais, 2018); the blue box is the Ngozi prospect zoomed in on the figure to the right; yellow circles are MT-TEM stations

resource has been discovered within the western branch, but high-temperature surface geothermal manifestations are prominent (see Figure 2) and more efforts are underway to discover and exploit geothermal resource for electric power generation and direct use. Apart from the volcanically hosted geothermal system which is located along the EARS, several low-medium (fault controlled) geothermal systems can be found in older rocks (Precambrian rocks and in Mesozoic sedimentary basins) in Tanzania (Figure 2).

2.2 Previous geothermal studies in Tanzania

Geothermal exploration in Tanzania dates back to 1949 when several reconnaissance surveys were carried out (Walker, 1969). Between 1976 and 1979, the Swedish company SWECO carried out exploration studies with the main focus being the regional sampling of the hot springs mainly in the northern part of the country and Mbeya region in the southwest (SWECO, 1978). During the SWECO exploration survey, 50 hot springs were studied with the purpose of exploiting the geothermal resources in Tanzania. The results indicated high-temperature resources in Lake Manyara, Lake Natron, Ngorongoro crater and the Mbeya region (see locations in Figure 2). In 1982, McNitt (1982) estimated the geothermal potential in the country and suggested that it could be as high as 650 MWe. Hochstein et al. (2000) reviewed some of the reconnaissance data and concluded that the geothermal resource in the country was small and limited. In 2005, DECON, SWECO and Inter-consult performed gravity and resistivity surveys in Songwe prospect and proposed a geothermal model and recommended further detailed studies (DECON et al., 2005). In 2014, JICA published a report on a data collection survey focused on geothermal development. Their volumetric assessment indicated that the total geothermal resource potential for Tanzania is 650 MWe (JICA, 2014). Based on natural heat flow discharge from the hot springs, Mnjokava (2014) and TGDC (2018) estimated the geothermal potential in the country to be about 5,000 MWe.

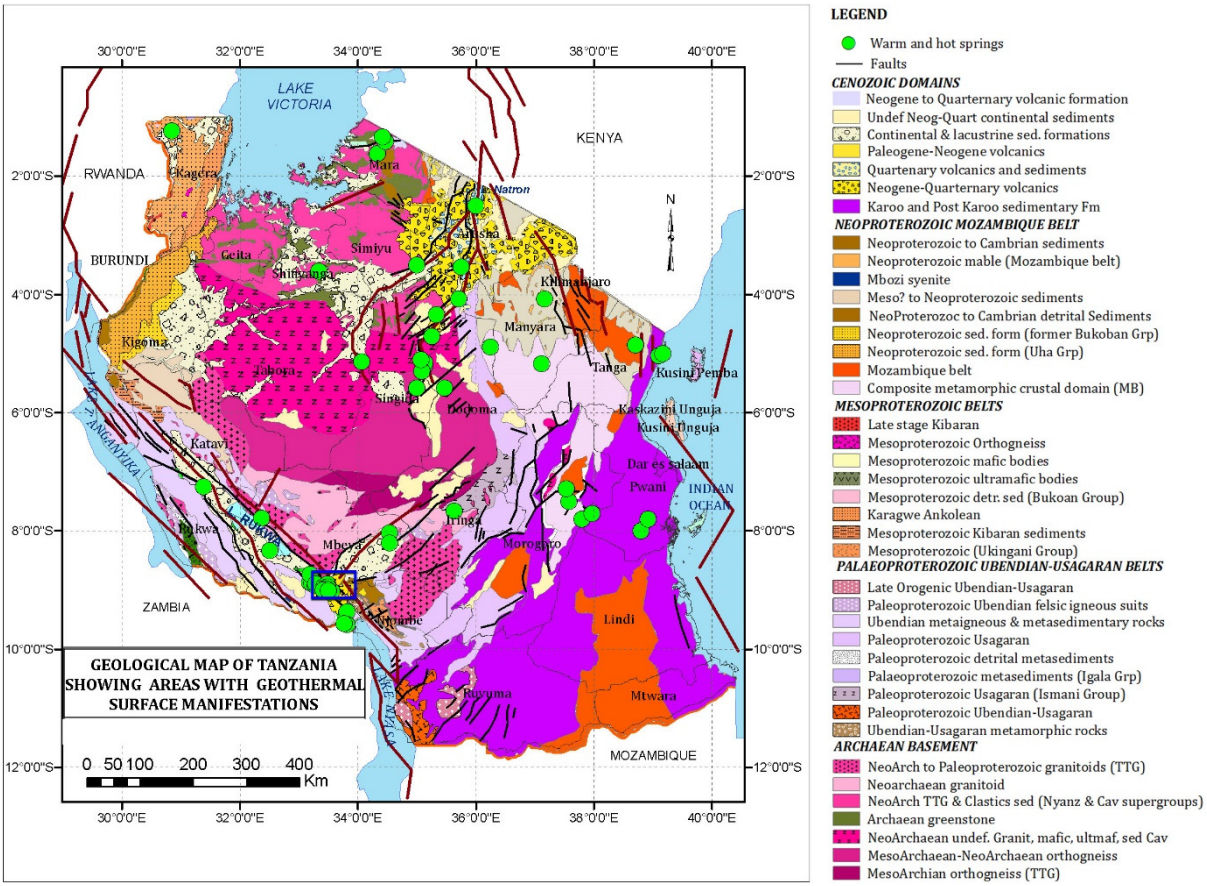

FIGURE 2: Geological map of Tanzania showing the location of Ngozi geothermal prospect (boxed in blue) at the triple junction of the EARS (red lines); the green circles are the surface geothermal manifestations. Map modified from Pinna et al. (2008)

Since 2015, Tanzania has been collaborating with several development partners including ISOR, UNEP/ARGEO and MFA/NDF (ICEIDA) to perform detailed surface exploration studies in 4 prospects namely Ngozi, Songwe, Mbaka and Luhoi (Alexander et al., 2016; ELC and TGDC, 2017) and assessment of areas for surface exploration studies (Hersir et al., 2015a). The results indicated that Ngozi is a high-temperature geothermal system with reservoir temperature greater than 230°C and an estimated resource of 140 MWe (Alexander et al., 2016). Mbaka-Kiejo was concluded to be a medium-temperature geothermal system with an estimated resource of 10 MWe (ELC and TGDC, 2017). Songwe prospect was regarded to be a medium-temperature, fault controlled geothermal system and Luhoi was concluded to be a low-temperature geothermal system with reservoir temperature less than 100°C hosted in Mesozoic sedimentary formation. In general, all the resources in the aforementioned prospects are to be tested by drilling with the first priorities being Ngozi and Mbaka-Kiejo prospects, located in SW-Tanzania.

2.2 The Ngozi geothermal prospect

2.2.1 Location of the study area

Ngozi geothermal area is located about 10 km southeast of Mbeya Town on the southern triple junction axis of the EARS within the Rungwe volcanic province (see Figures 1 and 2) which consists of four main volcanic eruption centers: Ngozi (2,620 m a.s.l.), Rungwe (3,000 m a.s.l.), Tukuyu (1,300 m a.s.l.) and Kiejo (2,200 m a.s.l.). The triple junction consists of three major rift basins, the Rukwa-Tanganyika Basin trending northwest (in the north), the less developed Ruaha-Mtera-Usangu depression trending

northeast (in the east) and the Karonga basin (Malawi rift) trending southeast which stretches to the south through Malawi and culminates in Zambia.

2.2.2 Geological and geothermal setting of Ngozi prospect

Ngozi volcanic centre is an uplifted (more than 2,500 m a.s.l.) elliptical structure forming a 2.5 km long, 1.6 km wide and 74 m deep caldera filled with water on top of the mountain (Josephat, 2016). This crater lake is classified as the second largest in the East African Rift and in Africa (Delalande et al., 2015). It was formed in Late Quaternary to Holocene (Fontijn et al., 2010a; Fontijn et al., 2012; Delalande et al., 2015) during an uplift caused by shallow intrusions of rhyolitic magma which episodically erupted depositing large volumes of volcanic pumice, scoria and other forms of pyroclastic rocks. This was accompanied by a series of small eruptive centres observed in the area as volcanic cones, domes and eruption craters resulted from the continental hotspots or plume activity (Ebinger et al., 1989; Delalande et al., 2015). The Ngozi volcanic system comprises the Ngozi dome as the central volcano with a collapse structure at its central forming a caldera filled with a mixture of magmatic (30-35%) and meteoric (70-65%) waters (Kraml et al., 2008; Alexander et al., 2016). A 4 km wide NW-SE trending fault zone whose eastern arm is partly mapped by surface data transects the Ngozi dome. Three hot springs connected by the N-S trending structures with temperature of 89, 78 and 66°C were mapped at the bottom of the lake (Kraml et al., 2008).

Generally, Ngozi and its surrounding areas are covered with varieties of rock types. Quaternary ash pumice resulting from ignimbrite volcanic eruptions within the last 1 ka (Fontijn et al., 2010b) covers an extensive area (Figure 3). Alluvial sediments deposited in depocentres on top of the basement or older volcanic rocks cover the low plains of Ngozi and are overlain by Quaternary ash pumice. The alluvial sediments disappear close to the dome area. It is likely that the surface had been uplifted, exposed and eroded during the dome stage about 10 ka ago or/and completely removed from a deeper surface during an episodic eruption phase up to 1 ka ago in the dome area and the spaces were occupied by the young volcanic rocks.

Ngozi prospect is characterized by three main sets of faulting trends; the NW-SE major trend, the NNE-SSW trend and the NE-SW structural trends, most of them mapped from remote sensing (Alexander et al., 2016). The northeastern and northwestern faults follow the current stress regime and are therefore interpreted to be young faults, reactivated due to stresses at the triple junction (Fontijn et al., 2010a). The northwest trending inferred fault which connects several eruption centres northwest and southeast of the Ngozi caldera and passes through the Lake has been observed in this study to be about 4 km wide forming a graben structure of about 7 km length engulfing the Ngozi caldera lake. This fault zone was interpreted by Fontijn et al. (2012) as a narrow NW-SE buried rift fault, dextral truncated by the NE-SW trending faults southeast of the Ngozi caldera.

The geochemical studies conducted so far consider the Ngozi area to be a high-temperature geothermal field based on data from three hot springs. Three hot springs with temperature of 89, 78 and 66°C were mapped at the bottom of the Ngozi Crater Lake (Kraml et al., 2008). The hot springs were of NaCl composition. Na-K geothermometry from the three hot springs in the lake (66-89°C) indicated a reservoir temperature of >230°C locally recharged by meteoric water from the Ngozi highlands through fractures, faults and possibly fissures (Ochmann and Garofalo, 2013). This observation is the most important geochemical evidence of the existence of a high-temperature geothermal system in the area.

Several hot springs of temperature ranging between 30 and 84°C are located northwest and southwest of the area and have different geochemical composition (Na-HCO_3) and properties. It has been concluded that they are heated through conduction, being discharged from the deep seated faults with reservoir temperatures ranging from 120 to 130°C (Josephat, 2016; Alexander et al., 2016). Petrographic studies of rock samples using XRD analysis indicate different clay minerals including kaolin, illite, smectite and other secondary minerals like calcite, quartz, epidote and zeolite. The presence of quartz, illite and epidote mineral assemblage indicates that the rocks were once exposed to the geothermal reservoir environment (Alexander et al., 2016).

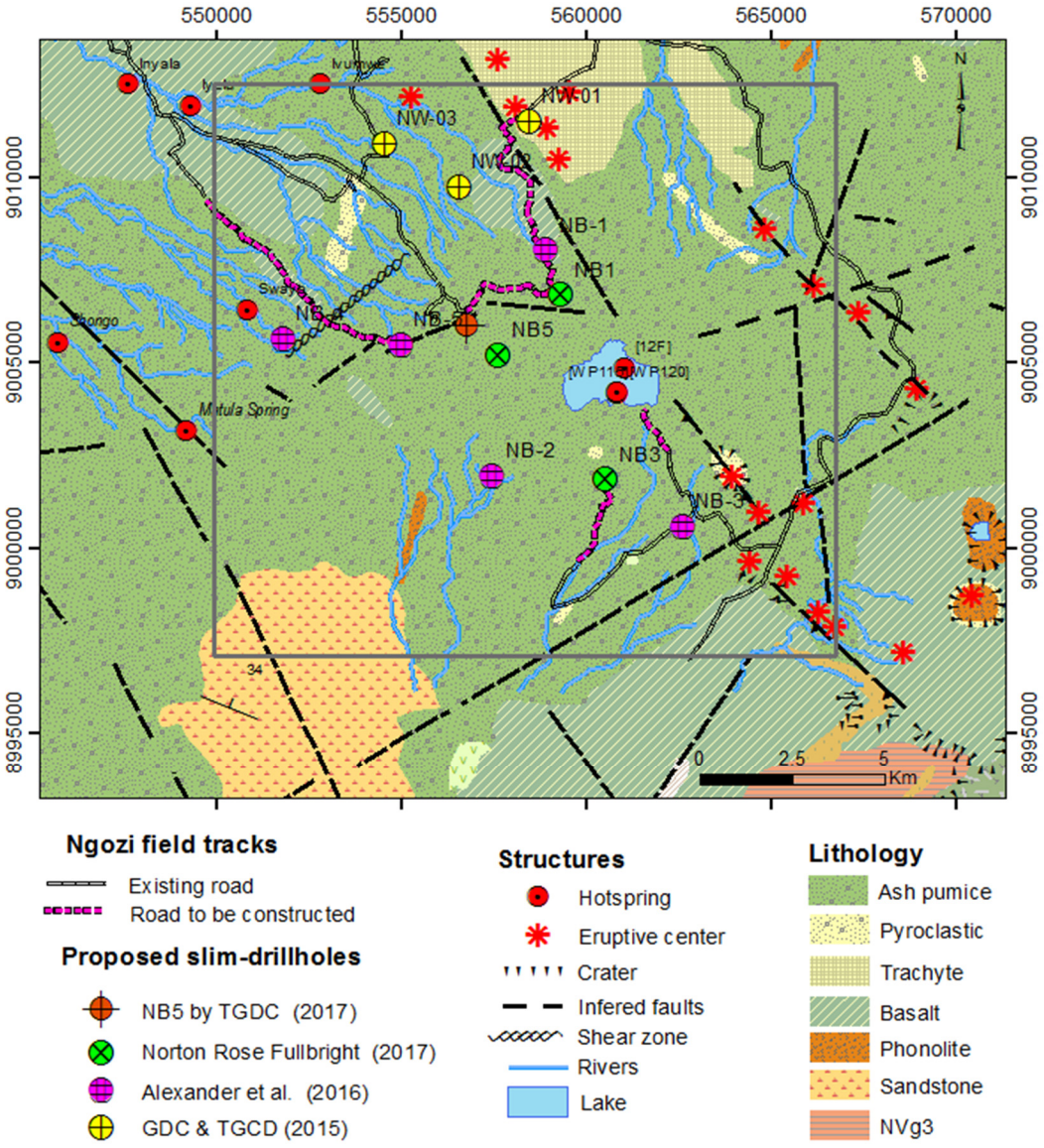

FIGURE 3: Geological map of the Ngozi geothermal prospect with tectonic structures and surface geothermal manifestation; map modified from Alexander et al. (2016), the grey box is the study area

2.3 Previous geothermal studies in Ngozi (general review)

Geothermal exploration studies in Ngozi prospect were conducted from 2006 to 2013 within the framework of GEOTHERMAL- technical corporation programme implemented by the Federal Institute of Geosciences and Natural Resources (BGR, Hanover, Germany) on behalf of the Federal Ministry for Economic cooperation and development and the government of Tanzania (Kraml et al., 2008; Kalberkamp et al., 2010; Ochmann and Garofalo, 2013). Earlier, there had been several academic research studies in the area (e.g. Ebinger et al., 1989; Delvaux et al., 1992; Ebinger et al., 1993; Delvaux and Hanon, 1993; Delvaux et al., 1998; Gibert et al., 2002), mostly focusing on the regional tectonic and volcanological evolution of the Western branch of the East African Rift System and volcanism of the Rungwe volcanic province at the triple junction. Major geothermal findings were first revealed during the GEOTHERMAL technical corporation programme (Kraml et al., 2008). The results included the first mapping of the three hot springs with temperature 89, 76 and 66°C located at the bottom of the

Ngozi caldera lake. The geochemical study concluded that the NaCl rich hot springs were discharging from the geothermal reservoir with a temperature of 232°C (based on Na-K geothermometry) located below the Ngozi caldera lake. However, the major conclusion from the study was that Ngozi and Songwe were a single geothermal system, Songwe being the outflow from Ngozi which was regarded to be the up flow.

Based on surface geological studies from 2006 to 2010, Delvaux et al. (2010) concluded that the Ngozi geothermal system was located between the Ngozi caldera and the Mbeya town. They suggested that the discharge area is in Songwe valley and the system is recharged from the Ngozi volcano area influenced by the strong altitude gradient. This meant that the proposed geothermal reservoir was located far northwest of the Ngozi caldera. A similar interpretation was done by Kraml et al. (2008) and Kalberkamp et al. (2010) based on the interpretation of a magnetic low from the regional aeromagnetic survey from Marobhe (1989).

These important conclusions were rejected by Alexander et al. (2016) based on the detailed integrated surface geological and structural mapping, geochemical studies (soil gas sampling, fluid gas sampling, and water chemistry from the hot/cold springs from rivers and shallow boreholes), ground magnetic and gravity surveys as well as co-located MT/TEM soundings. Alexander et al. (2016) concluded that Songwe and Ngozi are two different geothermal systems; Ngozi being a high-temperature volcanically hosted geothermal system with reservoir temperature of 232°C and Songwe being a low- to medium-temperature fault controlled geothermal system. The study also concluded that the hot springs at the bottom of the lake were discharging from the 232°C hot reservoir located below the Ngozi caldera. The shallow trachytic intrusive below the caldera was regarded as a potential heat source of the system. The chemical composition of the Ngozi hot springs and the lake water was saline while the warm and hot springs located west-northwest and in Songwe prospect were all $NaHCO_3$ rich. However, it was reported that most of the MT soundings showed strong 3D effects at depth. In the inversion, a 1D earth model was assumed. Therefore, in order to minimize the 3D effects, the low frequency part of the data (reflecting depths greater than 2 km) were chopped off and never used. This had a great effect as information on resistivity at greater depth was missing. Neither faults nor heat source could be mapped at these shallow depths from the MT soundings. Moreover, the correlation between the geological structures and resistivity anomalies were missing in the report by Alexander et al. (2016). The integrated conceptual model concluded that the geothermal system in Ngozi is constrained to the area below the caldera itself, but it may extend laterally to the west to a maximum distance of 2,500 m from the Ngozi caldera rim with 10% level of confidence (Alexander et al., 2016). Finally, Alexander et al. (2016) proposed four slim well drilling targets, all of them are located outside the optimum resource boundaries because that area would not be accessible using a conventional drilling rig.

In 2017, the Ministry of Minerals and Energy and Tanzania Geothermal Development Company, Ltd. (TGDC) on behalf of the Government of Tanzania contracted Norton Rose Fulbright consulting company to assess the potential geothermal resources in the top five prospects in Tanzania including Ngozi (Norton Rose Fulbright and Omenda, 2017). They recommended that the drilling targets proposed by Alexander et al. (2016) should be shifted closer to Ngozi caldera. TGDC sent a field crew to Ngozi and concluded that two wells (NB1 and NB5) out of the three could be shifted. Therefore, it was decided to reprocess and 1D invert the MT-TEM sounding data in this project and integrate the resulting resistivity model with the geochemical and surface geological data.

3. GEOTHERMAL EXPLORATION METHODS

This part of the report covers the surface exploration methods commonly used in geothermal exploration prior to drilling. The methods discussed include surface geological mapping, geochemical methods and surface geophysical methods.

3.1 Geological methods in geothermal exploration

In geothermal exploration, a geological survey is normally the first study performed in order to get some information about the surface features of the area. It is an important tool for mapping surface distribution of the lithology (rock types), the alteration and the surface manifestations, and for suggesting a possible heat source. Moreover, it is used to identify the structures, e.g. fractures, joints and faults that may be important conduits for fluid migration. This method is limited to surface observation. Hence, it does not give detailed subsurface information of the area. The geological studies are often integrated with the geophysical findings and interpreted jointly. When conducting a geological survey, the purpose, methodology and findings are reported as follows:

The purpose is to answer the following questions based on surface geological information: what temperature is to be expected, how big is the geothermal field, where to drill (high temperature and permeable fractures or formation in the reservoir)?

Methods: In order to answer the questions above, geological and in particular structural mapping (faults, fractures, dykes, alteration minerals, volcanology, volcanic history, hydrogeology etc.) is carried out in the area, mapping of surface geothermal manifestations and integration of aerial photos, satellite images and drone images. Mapping of soil temperature and CO_2 soil gas flux and radon surveys may also be included to identify permeable zones leaking gases from the subsurface geothermal system.

Outcome: Three outcomes are normally expected from the geological studies, namely maps and cross-sections, a preliminary conceptual model (showing the possible upflow/outflow zones, depth to the heat source) and a report. However, the geological method is limited to direct observations on the surface and does not probe deep into the earth's crust.

3.2 Geochemical methods in geothermal exploration

The role of geochemical studies at the geothermal investigation/exploration stage is to analyse the subsurface composition of the reservoir fluids, estimate the fluid temperature in the reservoir and evaluate subsurface processes within the reservoir such as boiling or mixing. This is done by sampling and analysing the geothermal fluids of the reservoir that have been discharged to the surface through faults and fractures. The analytical results from the fluid samples (water and gas samples) can be used to predict the temperature of the reservoir (through chemical geothermometry studies), equilibrium state, salinity, gas content of the reservoir fluid, recharge/origin of fluid and flow directions (through isotopic studies) of the fluid. The geochemical results are always integrated with the geological and geophysical results to generate a conceptual model.

Like geology, geochemical methods are also limited to surface observations. In the current study previous geochemical results in the area are integrated with the current geophysical results to constrain the geothermal model of the area.

3.3 Geophysical methods in geothermal exploration

Unlike geological and geochemical methods, geophysical methods utilize equipment that measures directly physical parameters at the surface that are directly created by physical properties or processes at depth in the earth's crust (e.g. the resistivity of the rocks in the subsurface). Geophysical methods are divided into two categories: direct methods which are directly related to the reservoir (for instance, temperature and resistivity measurements) and structural methods also called indirect methods which include gravity, magnetics and seismics. The primary aim of geophysical exploration in any area of study is to:

- Delineate the geothermal prospect;

- Outline the drilling field (the size of the area);
- Locate a geothermal reservoir/aquifers and site wells; and
- Estimate the properties of the geothermal system such as permeability, temperature and alterations.

In geophysical exploration, the physical properties that are different from the surrounding rock create an anomaly in the measurements. This anomaly can be related to the geothermal system that is targeted. The aim of geophysical studies is to locate these anomalies.

3.3.1 Indirect geophysical methods (structural methods)

Structural methods describe structures such as fractures, faults, dykes or other forms of intrusions which are not necessarily related to the geothermal system. These methods include gravity, magnetic and seismic surveys (both active and passive seismics methods can be used).

3.3.2 Direct geophysical methods

Direct geophysical methods measure subsurface anomalies which are directly related to the geothermal system in the area of investigation. These methods include subsurface heat measurements and resistivity surveys.

4. RESISTIVITY METHODS

4.1 Resistivity methods in geothermal exploration

Resistivity methods are the most powerful geophysical prospecting method in geothermal exploration and the main method used for delineating geothermal resources. This is because the method measures/detects the resistivity anomalies of the subsurface rocks, which are directly related to the geothermal system in the area of investigation.

4.2 Resistivity of rocks

The electrical resistivity is defined through Ohm's law:

$$\boldsymbol{E} = \rho \boldsymbol{j} \tag{1}$$

where $\boldsymbol{E}$ = Electrical field [V/m];
ρ = Electric resistivity [Ωm]; and
$\boldsymbol{j}$ = Current density [A/m^2].

In geothermal fields, the resistivity of rocks is affected by salinity (in pore fluid), temperature of the pore fluid, porosity of the rock, saturation level of the pores, alteration of the rock and degree of melting of the host rock (Árnason et al., 1987; Hersir and Árnason, 2009).

4.2.1 Porosity, permeability and pore-structure of the rock

Resistivity decreases with increasing porosity of the host rock and increases with decreasing porosity as described in *Archie's law* (Archie, 1942):

$$\rho = \rho_w a/\Phi^n \tag{2}$$

where Φ = Porosity in proportions of total volume [0-1];
ρ_w = Resistivity of the pore fluid [Ωm];
ρ = Bulk resistivity [Ωm];

a ≅ 1; and
n ≅ 2

4.2.2 Salinity of the water in the rock pore spaces

Resistivity decreases linearly with increasing salinity of the pore fluid and increases linearly with decreasing salinity in the pore fluid; ρ ≈10/Concentration (Keller and Frischknecht, 1966).

4.2.3 Temperature (in pore fluid)

At moderate temperatures (0-200°C), resistivity of an aqueous solution decreases with increasing temperature due to increasing mobility of the ions caused by a decrease in viscosity of the pore fluid (Dakhnov, 1962). However, at temperature above 300°C, the same process increases fluid resistivity (Quist and Marshall, 1968).

From Dakhnov's relationship it can be seen that:

$$\rho_w = \rho_{WO}/(1 + \alpha(T - T_0)) \quad (3)$$

where ρ_w = Fluid resistivity at temperature, T [Ωm];
ρ_{wo} = Fluid resistivity at T_o [Ωm]; and
T_o = Reference temperature [°C].

4.2.4 Water-rock interaction and alteration mineralogy of the host rock

Alteration mineralogy controls the subsurface resistivity structure in high-temperature areas where the host rocks are volcanic. A shallow lying conductive cap is found in these areas with considerable amounts of conductive alteration minerals like smectite and zeolite that have a high cation exchange capacity (CEC) (Flóvenz et al., 2012). Below a core of high resistivity (geothermal reservoir) is reached (Figure 4). The transition from the low-resistivity cap to the high-resistivity core coincides with a change in mineral alteration, that is from smectite and zeolite to mixed-layered clays, chlorite and epidote which occurs at temperatures close to 230°C in basaltic geothermal systems (Kristmannsdóttir, 1979). The difference in conductivity between the smectite/zeolite and the chlorite/epidote alteration zones is

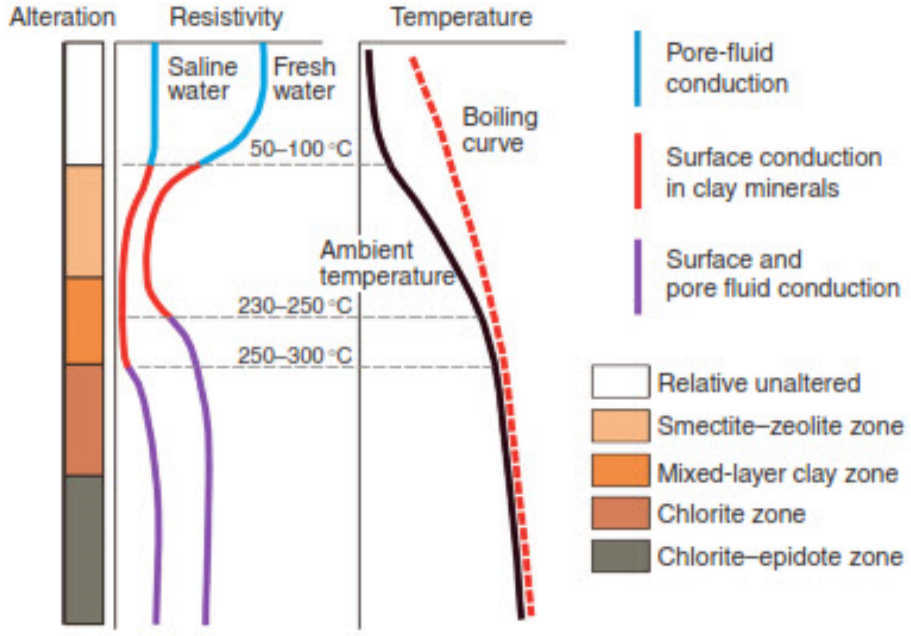

FIGURE 4: The generalized resistivity structure of a high-temperature geothermal field in volcanic environment (Flóvenz et al., 2012, modified from Flóvenz et al., 2005)

attributed by the difference in CEC. Smectite/zeolite have a higher CEC (0.8-1.5 meq g^{-1}) than the chlorite-epidote (0.01meq g^{-1}), hence, conductivity is higher in the cap than in the resistive core which is dominated by chlorite/epidote alteration mineralogy (Flóvenz et al., 2012). In a silica rich environment, the smectite, which is typically lower in CEC (often around 0.2-0.30 meq g-1) than that of smectite, tends to be replaced by illite at lower temperature (180°C) (Chi and Browne, 1991; Flóvenz et al., 2012). The relationship between the subsurface resistivity, hydrothermal alteration, temperature and conduction mechanism is summarized in Figure 4. It is important to note that the altered rocks tend to preserve the resistivity anomalies even if they have cooled down since the alteration process took place. Thus, finding the resistivity anomalies of a typical high-temperature geothermal system does not guarantee the existence of a hot geothermal system (Flóvenz et al., 2012).

4.2.5 Saturation level of the pores

Resistivity decreases with increasing saturation of the pores and increases when the pores are not saturated. For example, rocks below the groundwater table have low resistivity values because the pores are filled with water while rocks above water table have higher resistivity values because the pores are less saturated or dry. Geothermal systems are regarded as water saturated.

4.2.6 Melting of rocks (partial melt)

Partially melted rocks have lower resistivity because the high temperature (> 800°C) which causes the melting also increases mobility of the ions.

4.3 Main conduction mechanisms

Conduction in geothermal fields is dominated by three main mechanisms: mineral conduction, pore fluid conduction and surface conduction.

Mineral conduction is the conduction along the rock matrix itself. In geothermal systems, the rock matrix has very low to extremely low conductivity. At reservoir temperature, rocks normally function as an insulator. However, at very high temperatures (> 800°C) close to partial melting, the conductivity of the rock matrix becomes significant.

Pore fluid conduction is the conduction by dissolved ions in the pore fluid. This type of conduction mechanism is dominant in geothermal reservoirs where fluid occupies the cracks, fractures or pore spaces of the formation.

Surface conduction is caused by highly mobile ions (absorbed ions on the pore-surface) that form a conductive layer on the surface of the pore walls. This type of conduction mechanism is dominant in the smectite clay cap where the free ions absorbed at the walls of the altered rock unit are highly conductive. The high conduction in smectite is caused by its high CEC (Kristinsdóttir et al., 2010). In geothermal fields, the CEC is high within the smectite alteration zone (clay cap) and low in the chlorite-epidote zone (reservoir). Rock forming minerals in volcanic environment have practically no CEC, hence very low conduction (Kristinsdóttir et al., 2010). For details on surface conductivity the reader is referred to Flóvenz et al. (2012) and references therein.

5. MAGNETOTELLURIC (MT) METHOD

The magnetotelluric (MT) method is a natural source electromagnetic method using frequencies from several hundreds of Hz to less than 0.001 Hz. It can probe the earth and measure electrical resistivity to depths of several tens to hundreds of kilometres (Chave et al., 2012). It is this capability of penetrating

deep into the subsurface that makes it the only method to study deep resistivity structures (Jones, 2008). In MT surveys, the fluctuations in the natural electric field, **E,** and magnetic field, **B**, which are measured in orthogonal directions at the surface, allow us to determine the electrical resistivity distribution of the earth at depth.

5.1 MT source field

5.1.1 Main MT source field of high and low frequencies of the natural magnetic field spectrum

The low frequencies (<1 Hz) are generated by ionospheric and magnetospheric currents caused by the solar wind (plasma) which is emitted from the sun and interferes with the earth's magnetic field (Figure 5). The high frequencies (>1 Hz) are generated by lightening discharges mainly from the equatorial regions which propagate around the world within a waveguide bound to the ionosphere and the earth's surface (Chave et al., 2012).

5.1.2 MT field intensity variations with latitude

The intensity of the natural MT field varies with latitude. At the equator the high frequency waves are strong while at polar latitudes the low frequency waves are strong (Chave et al., 2012). This is because regular strong lightening discharges generate high frequency (> 8 Hz) electromagnetic waves in the equatorial regions while at the polar region large geomagnetic variations occur during magnetic storms which produce low-frequency signals caused by sporadic increases in the rate at which plasma is injected from the sun (see Figure 5).

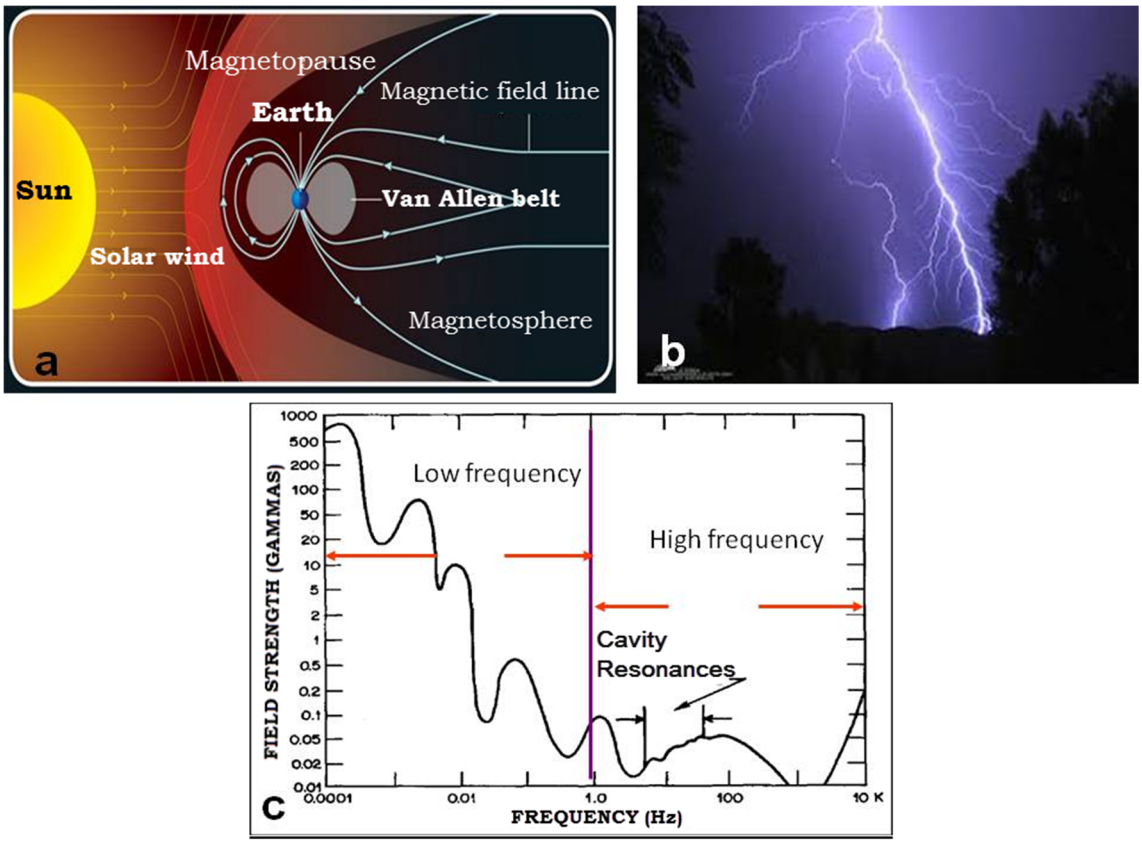

FIGURE 5: a) Source of electromagnetic field; b) Solar wind interaction with magnetosphere; and c) Natural magnetic field spectrum (SOHO, 2010)

5.2 The basic electromagnetic theory and governing equations

The theory of electromagnetic induction is described by Maxwell's equations as shown below (Chave et al., 2012). The four Maxwell equations are a complete description of the relationship between electric and magnetic fields in any medium:

$$\boldsymbol{\nabla \cdot D} = \eta \tag{4}$$

$$\boldsymbol{\nabla \cdot B} = 0 \tag{5}$$

$$\boldsymbol{\nabla x E} = -\frac{\partial \boldsymbol{B}}{\partial t} \tag{6}$$

$$\boldsymbol{\nabla \times H} = \boldsymbol{J} + \frac{\boldsymbol{\partial D}}{\boldsymbol{\partial t}} \tag{7}$$

where $\boldsymbol{B}$ = Magnetic Induction [T];
$\boldsymbol{H}$ = Magnetic field intensity [A/m];
$\boldsymbol{D}$ = Electric displacement [C/m^2];
$\boldsymbol{E}$ = Electrical field intensity [V/m];
η = Electric charge density of free charges [C/m^3]; and
$\boldsymbol{J}$ = Electric current density [A/m^2].

Equation 4 states that the electric field diverges from electric charges, the net outflow of the electric field through any closed surface is proportional to the charge enclosed by the surface (Gauss's law of electricity); Equation 5 says that there are no magnetic monopoles (Gauss's law of magnetism); Equation 6 states that circulating electric fields are produced by time varying magnetic fields (Faraday's law); and Equation 7 that circulating magnetic fields are produced by the vector sum of electric currents and time varying electric fields (Ampere's law).

It can be shown that the relationship between the electric and magnetic fields in any given media can be expressed by the following equation:

$$\begin{bmatrix} Ex \\ Ey \end{bmatrix} = \begin{bmatrix} Zxx & Zxy \\ Zyx & Zyy \end{bmatrix} \begin{bmatrix} Hx \\ Hy \end{bmatrix} \tag{8}$$

or in matrix notation:

$$\boldsymbol{\vec{E} = Z\vec{H}} \tag{9}$$

where, $\boldsymbol{\vec{E}}$ = Electric field vector;
$\boldsymbol{\vec{H}}$ = Magnetic field vector; and
$\boldsymbol{Z}$ = A complex impedance tensor which contains information on the subsurface resistivity structure.

5.3 Skin depth – "depth of penetration"

An estimated quantitative measure of the penetration depth of a wave in a conductive medium can be expressed by Equation 10. The depth of penetration increases with increasing period, *T,* and increasing resistivity in the subsurface. The depth of penetration is called the "skin depth". This means that a resistive media can be investigated to much greater depth than a conductive media:

$$\delta \approx 500\sqrt{\rho T}\ [m] \tag{10}$$

where δ = Skin depth or "depth of penetration" [m];
ρ = Apparent resistivity [Ωm]; and
T = Period [s].

5.4 Homogeneous earth

In a homogeneous earth, electromagnetic waves propagate such that the electric and magnetic fields are orthogonal and the ratio of the electric to the magnetic fields is directly related to the apparent resistivity of that media. The relationship is given by the following equation (Keller and Frischknecht, 1966):

$$\rho_a(T) = 0.2T \left|\frac{Ex}{By}\right|^2 \quad (11)$$

Depending on how the parameters vary, the half space earth can be explained by three types of resistivity models which include 1D, 2D and 3D and are explained in the following sub-chapters.

5.4.1 1D earth

The layered earth model (Figure 6) assumes that the half space earth is flat, composed of many layers and each layer is characterised by a uniform conductivity, permeability and permittivity (Ward and Wannamaker, 1983).

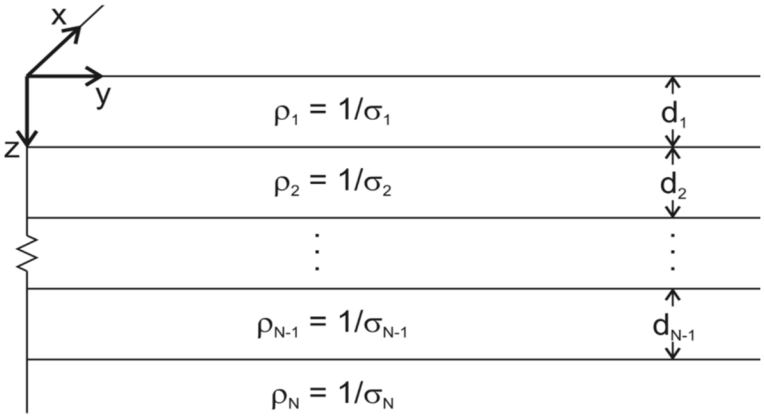

FIGURE 6: N-layered earth model showing resistivity variations with depth

In 1D interpretation, it is assumed that the resistivity varies only with depth. Thus, the diagonal elements of the impedance tensor, *Zxx* and *Zyy* (which couple parallel electric and magnetic fields components), are zero while the off-diagonal components (which couple orthogonal electric and magnetic field components) are equal in magnitude but have opposite signs (Flóvenz et al., 2012; Chave et al., 2012).

5.4.2 2D earth case

In 2D interpretation it is assumed that resistivity varies along one of the two principal horizontal directions as well as with depth. In a 2D earth case, *Zxx* and *Zyy* are equal in magnitude but have opposite signs while *Zxy* and *Zyx* are different (Chave et al., 2012).

5.4.3 3D earth case

The real earth is best described by a 3D model where resistivity varies in all three directions ($\rho(x, y, z)$). In a 3D earth model all the components of the impendence tensor are non-zero and the diagonal elements of the impedance tensor *Zxx* and *Zyy* do not vanish simultaneously in any coordinate system. Likewise, the non-diagonal elements of the impedance tensor *Zxy* and *Zyx* differ. Thus, when interpreting a 3D earth model, all tensor elements are considered (Chave et al., 2012).

5.5 Problems in MT measurements

5.5.1 The "Dead band" problem

The so-called **"**Dead band" in MT is the frequency band between 0.5 and 5 Hz of the EM power spectrum (see Figure 7). This band is characterized by low-amplitude signals. It is caused by the interaction between the earth's magnetic field generated by magneto-hydrodynamic processes within the earth's outer core and extra-terrestrial magnetic fields generated by the solar wind in the ionosphere

that MT soundings seeks to exploit. It is attributable to the inductive source mechanisms, one effective above ~1 Hz, the other below ~1 Hz, and is frequently manifested in MT sounding curves by a reduction in data quality (Chave et al., 2012; Flóvenz et al., 2012). Unfortunately, the remedy for this problem in MT data is not yet discovered. Thus, the processed data are always of low quality in the dead band frequency range.

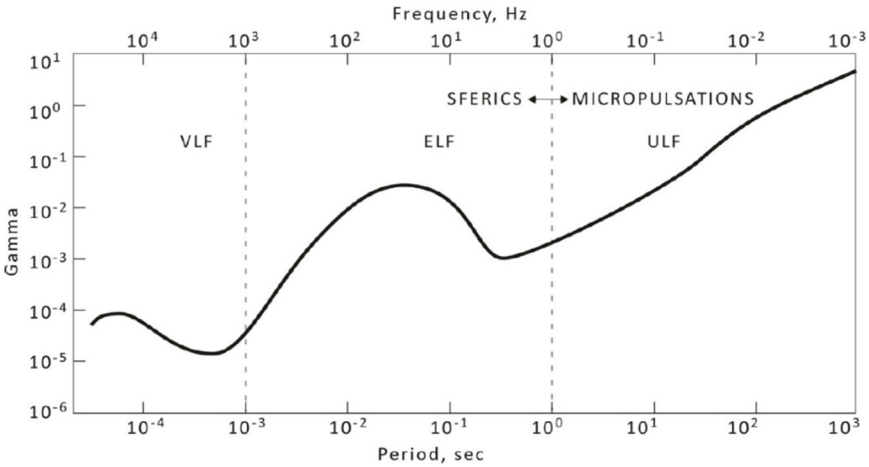

FIGURE 7: The mean natural magnetic field amplitude spectrum in gammas ($\gamma=nT$) as a function of the period (Flóvenz et al., 2012)

5.5.2 MT static shift problem and correction techniques

Static shift in MT is caused by shallow resistivity heterogeneities close to the sounding site and manifests itself in parallel shift of the apparent resistivity over the whole range of frequencies (Park and Livelybrooks, 1989). Thus, the correct level of the apparent resistivity curve may be located above, below or between the measured responses. This problem has been frequently reviewed by several authors and it has been suggested to use an independent measurement for the shallow resistivity as a correction (e.g. Sternberg et al., 1988; Bahr, 1990; Cumming and Mackie, 2010; Árnason, 2015). Despite the strong effects on the resistivity curve, static shift does not affect the phase curve (Jones and Groom, 1993). Due to the static shift problem the apparent resistivity is distorted by a multiplicative constant, *S*. If the static shifts are not corrected for, the inversion models may contain structures that could mislead the interpretation. The theory of the physics of distortion of both the electric and magnetic fields from charges at resistivity boundaries has been understood and its application in MT is well described by Chave and Smith (1994). Chave et al. (2012) described the possible processes which cause static shift in MT measurements. These include current distortion, topographic effect and electric field or voltage distortion. The use of TEM data co-located with MT soundings corrects these distortions (Pellerin and Hohmann, 1990). This technique is performed by joint inversion of co-located MT-TEM sounding pairs as discussed in Section 8.

Topographic effect. This kind of distortion is common in areas with rough topography like volcanic areas. In such areas the electric currents tend to concentrate beneath the depressions and disperses under peaks. Hence, the electric field increases in valleys and decreases on the hills. Measuring MT fields in such areas, the MT response signals will be higher in the valleys and lower on the hills, hence results in upward and downward shifts, respectively. For the apparent resistivity curves, this can be noticed as static shifts.

Current distortion is caused by electric charge distributions accumulated on the surface of a shallow conductor. This distortion is due to deviations in regional current flow as it encounters a conductive anomaly in the subsurface (Jones, 1983). Here, the currents are channelled into a conductive anomaly and abruptly diverged from a resistive anomaly and vice versa (see Figure 8).

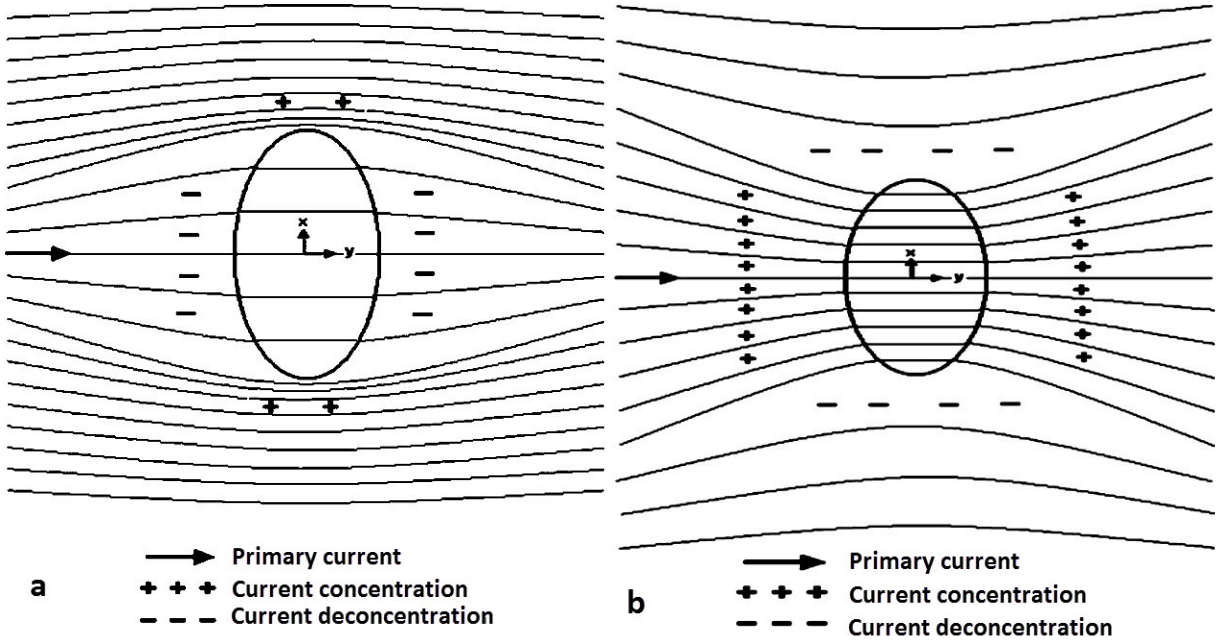

FIGURE 8: Current channelling due to inhomogeneous conductivity showing; a) Flow-around effect in the vicinity of a resistor; and b) Current-gathering effect in a conductive inclusion (Jones, 1983)

5.5.3 Cultural noise problem and remote reference

In MT surveys the measured signal is composed of signal and noise. Part of the noise is cultural noise (noise caused by local activities within or close to the sounding site e.g. power lines, factories, activities that cause ground shacking etc.). In order to reduce the effect of the cultural noise and increase the signal to noise ratio, MT data from a remote reference station (ca. 30 km distance) at an electronically quiet site such that the cultural noise is uncorrelated between the two sites is used. The station data and remote reference data are processed together, which has been proven to considerably increase the signal to noise ratio (Gamble et al., 1979; Clarke et al., 1983).

5.6 Instrumentation and acquisition field layout

The electric and magnetic field time series used in this study were acquired in the frequency range between 10000 Hz and 0.0001 Hz using three broadband Phoenix MTU V5 systems (Phoenix, 2018); five channels, 2 electric field channels Ex and Ey and 3 magnetic field channels Hx, Hy and Hz (Figure 9). The instrument has a dynamic range of 130 dB with a power line notch filter of >40 dB plus selectable low pass, high pass and band bass filters. The acquisition field lay out is shown in Figure 10.

FIGURE 9: Phoenix V5 2000 MT system (Phoenix, 2018)

5.7 Data processing (time series analysis)

MT data were processed using a combination of different workflows described in Phoenix' MT processing manual (Phoenix, 2005):

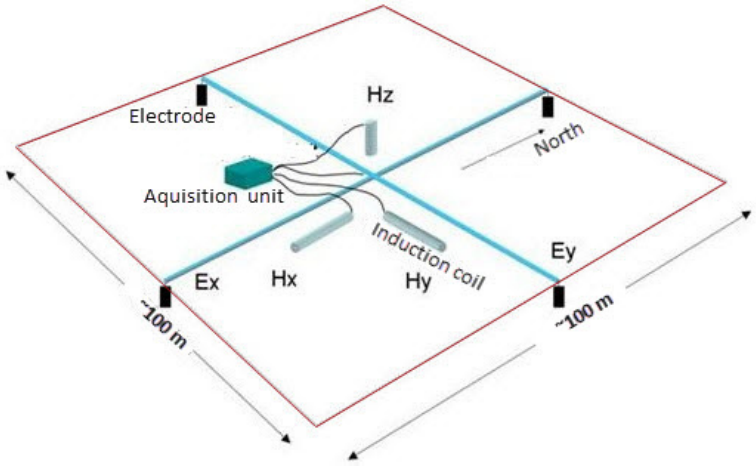

FIGURE 10: The field setup of an MT sounding (Openei, 2018)

i. Viewing the time series data using Synchro Time Series view program. This program allows graphical viewing of the time series and has an option of printing computed power spectra density and coherence between pairs of orthogonal channels.
ii. Decimation of the time series data as described by Wight et al. (1977) and Wight and Bostick (1980) through visual inspection to recognize and exclude noisy data from the records.
iii. The conversion of the decimated time series data into frequency domain using Fast Fourier Transformation method (Bendat and Piersol, 1971) in Phoenix's SSMT2000 software. This produces the Fourier coefficients (parameter) which can then be used to calculate high and low frequency MT plot files (MTH, MTL) with multiple cross powers for every frequency.

5.7.1 Data processing - edi file format

The computed high and low frequency MT files (MTH, MTL) from SSMT2000 were used as input files for the MTEditor software. In MTEditor the resistivity and phase for every frequency were edited. The editing is either done automatically or manually. The edited files were saved as .mpk files and finally exported to an industry standard edi file (electronic data interchange) suitable for use with other geophysical inversion softwares like TEMTD or WinGLink where joint inversion with TEM data is performed.

5.7.2 Choosing a resistivity invariant

In 1D inversion, several invariants exist and the question arises which apparent resistivity curve to invert for. This is discussed by Park and Livelybrooks (1989). Three types of average, determinant, arithmetic average and the geometric mean, were computed (Figure 11) and compared as described in Park and

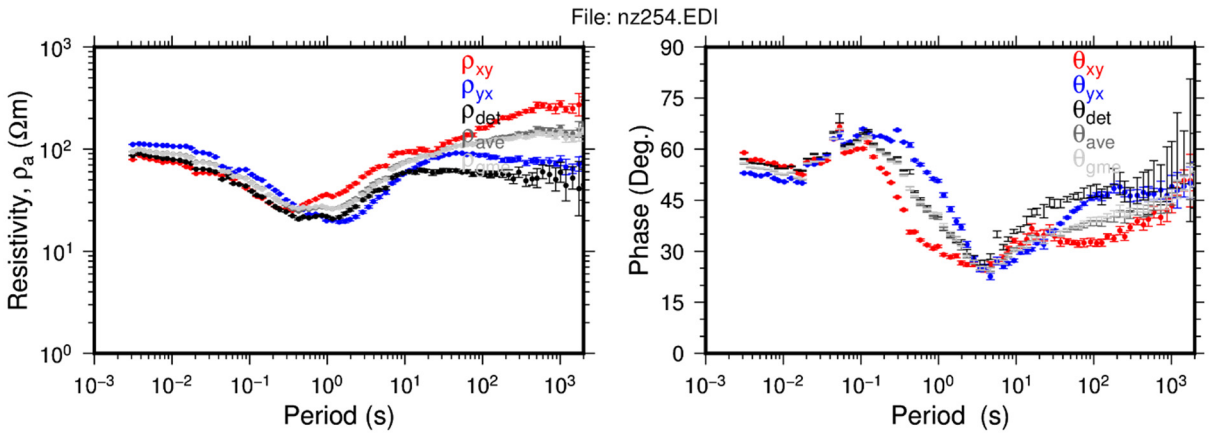

FIGURE 11: Processed data for sounding nz254 - apparent resistivity and phase curves for different parameters. All the invariant parameters were different. Note how the determinant visually matches "a local 1D resistivity model" but deviates for periods above 10 s

Livelybrooks (1989). The arithmetic mean invariant parameter was chosen over the determinant and the geometric mean because it yielded stable and reasonable estimates of the ρxy and ρyx resistivities for each MT station see Figure 11 and Appendix I in Didas, 2018). According to Park and Livelybrooks (1989), the determinant (det), the geometric mean (gm) and the arithmetic mean (ave) give the same value for a 1D response. For 2D earth, the det and gm were reduced to the same value but the ave was different. For 3D earth, all these parameters were different. Based on the Park and Livelybrooks (1989) descriptions, it was observed that most of the stations used in this study at shallow depths (high frequency) are well explained by a 1D model but at greater depths either a 2D or 3D model describe the features better. However, there were few stations, which could be well described by a 1D model throughout the frequency range. The determinant invariant which has been commonly used in MT inversion at ISOR and suggested by Park and Livelybrooks (1989) does not work for the Ngozi MT data presented in this report.

6. TRANSIENT ELECTROMAGNETICS, TEM METHOD

Transient Electromagnetics, TEM method (also known as Time Domain Electromagnetics, TDEM), is a geophysical exploration technique which detects subsurface electrical resistivity properties. In TEM, electric and magnetic fields are induced by transient (short time varying) pulses of an electric current in a loop or dipole and the subsequent decay response is measured. The decay response measured in the TEM receiver is the magnetic field created by the eddy currents in the subsurface.

6.1 TEM source field

When applying the TEM method, a controlled and time varying man-made magnetic field is used to induce currents into the earth. Unlike the MT method, TEM is an active method where the primary magnetic field is known.

6.2 The transient electromagnetic theory and governing equations

The basic principle of TEM is governed by Faraday's law of induction and Lenz's law of magnetism which are described in detail by Árnason (1989). For TEM measurements the source is either a loop or a dipole. In this project, the so-called central-loop TEM method is described and applied. In that set-up the receiver is at the centre of the loop source (Figure 12). A direct current from a controlled source is fed into a loop of wire and is regularly turned off in short time intervals. According to Faraday's law, once the current in the loop is turned off, a nearly identical current is induced in the subsurface to preserve the magnetic field produced by the original current (eddy current). Due to ohmic losses, the induced currents cause a change in the magnetic field which induces subsequently new eddy currents. The net result is a downward and outward diffusion of currents in the subsurface.

6.3 Depth of penetration

TEM measurements allow geophysical exploration from a few metres below the surface to several hundreds of metres depth (see Árnason, 1989 for detailed mathematical expression**)**. The depth of penetration in TEM surveys depends on the subsurface resistivity, current induced, receiver sensitivity, and transmitter-receiver geometry (size of the transmitter loop).

6.4 Instrumentation and data acquisition

The TEM survey setup consists of a transmitter, transmitting coil or wire, receiver coil or antenna, and a receiver (see Figure 12.). The data acquisition in TEM measurements works as shown in Figure 12. A

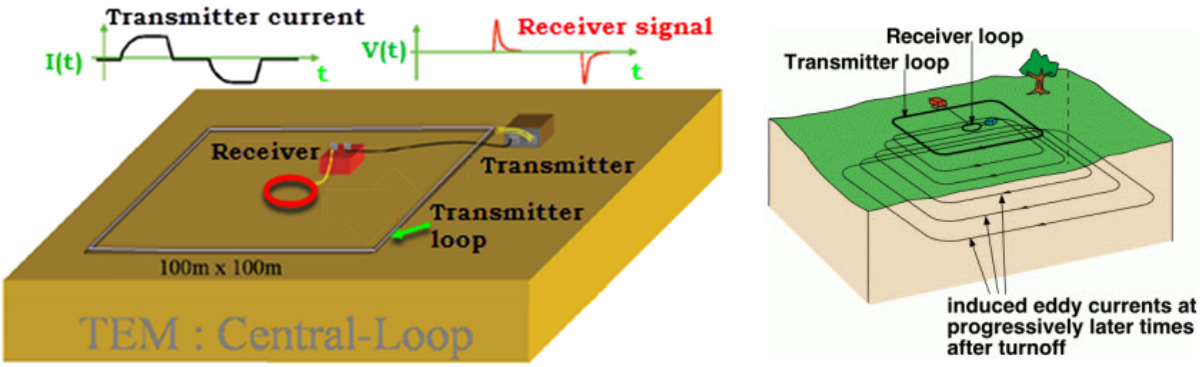

FIGURE 12: TEM field layout demonstrating how it works (Zonge, 2018)

current is injected into a transmitter wire loop (normally 100 m × 100 m or a large loop) which generates a magnetic field. Prior to data acquisition, the transmitter and the receiver are synchronized so that the receiver knows when the transmitter turns off the current. The receiver must also know the time it takes to turn off the current. The current in the transmitter loop is regularly switched on and off at equal time intervals. The magnetic field around the wire loop induces weaker eddy currents immediately below the transmitter loop, approximating a mirror image. As the initial near-surface eddy currents decay, their magnetic field in turn induces weaker eddy currents at greater depths which also decay. The process continues while currents weaken as depths increase.

The magnetic field created by the eddy currents in subsurface is then measured by the TEM receiver. The measurements of the magnetic field are done while the transmitter current is turned off. Measurements are typically made in the time range from 10 μs to 10 ms at 20 to 30 discrete time gates or time intervals following the turn-off of the current.

The magnitude and rate of decay of the induced currents depend on the conductivity of the subsurface and geometry of the medium which they propagate through. In conductive media the currents will decay more slowly while in resistive media decay is faster. In cases where a conductive layer lies between two resistive media, the current will be trapped and decay slowly in the conductor while decaying more rapidly in the surrounding resistive layers. However, for deeper investigation of the subsurface in conductive media, the measurement time can be extended to up to 1 s.

In this study, 64 TEM sounding data were collected by using Zonge GDP32[24] TEM equipment (Zonge, 2018) using a 100 m × 100 m square transmitter loop and a central receiver, measuring the vertical component of the magnetic field. The data are processed and jointly inverted with MT data to generate a 1D Occam model.

6.5 Data processing (raw data analysis) using TemX program

Prior to modelling, the raw TEM data were converted to *.USF file format by using the software made available by the instrument manufacturer. The *.CAC files produced by the Zonge receiver were converted to *.AVG format by the 'TEMAVGW" program and then to *.USF format by the "TEMTRIM" program. The *.USF files are the input files for the TemX program created at ISOR (Árnason, 2006a). The TemX program reads and processes the standard file formats of the central loop TEM data. It performs normalization of the voltages with respect to the transmitted current, gain and effective area of the antenna and then displays all the data graphically, allowing the user to omit outliers, it calculates averages of the data set and the time apparent resistivity. The program produces an output file *.inv ready for inversion in programs such as TEMTD which is explained in the following chapter.

7. THE TEMTD 1D INVERSION PROGRAM

7.1 Inversion of resistivity data using TEMTD program

TEMTD is a 1D inversion program which uses a horizontally layered earth model for central square-loop TEM and MT data. The program was developed at ISOR in 2006 (Árnason, 2006b). It can be used to invert separately TEM or MT data or jointly. The TEMTD software is written in ANSI-C, runs under UNIX/LINUX operating systems and uses the gnuplot graphics programme for graphical display during the inversion process. The program can be used to perform both layered inversion and minimum structure (Occam) inversion of which the fixed thickness of the layers increases exponentially with depth. In this project Occam inversion was used.

7.2 The general concept of inversion

The inversion algorithm used in TEMTED is based on the Levenberg-Marquardt non-linear least square inversion as described by Árnason (1989). The misfit function is the root mean square difference between the measured and calculated values (chi-square), weighted by the standard deviation of the measured value. The program solves for resistivities and thicknesses of discrete layers and uses both amplitude and phase as input. During inversion the program offers the possibility to keep models smooth with respect to resistivity variations between layers and layer thicknesses. Moreover, it provides options for applying a damping factor which counteracts sharp steps and oscillations in the model values. The function that is minimized is the potential given by the equation below:

$$\mathrm{Pot} = \mathrm{X2} + \alpha \cdot \mathrm{DS1} + \beta \cdot \mathrm{DS2} + \gamma \cdot \mathrm{DD1} + \delta \cdot \mathrm{DD2} \qquad (12)$$

where, DS1 and DS2 are the first and second order derivatives of log-conductivities in the layered model and DD1 and DD2 are the first and second order derivatives of the logarithms of the ratios of layer depths. The coefficients α, β, γ and δ are the relative contributions of the different damping terms and are specified by the user.

8. 1D JOINT INVERSION OF MT AND TEM DATA FROM NGOZI PROSPECT

MT/TEM data used in the inversion were collected in three survey campaigns by: BGR in 2008-2013 (MBY* stations), TGDC and GDC in 2015 (ng* stations), and TGDC in 2016 (nz* stations). The location of the soundings is shown in Figure 1. A total of 64 MT/TEM soundings are used for interpretation. MT sounding data by the BGR were acquired using Metronix MT units and TEM sounding data were acquired using Geonix-7 units. The other MT and TEM sounding data were acquired using the 5-channel MT data acquisition system (MTU-5A) from Phoenix Geophysics and TEM data were acquired using Zonge GDP32[24] TEM equipment using a 100 m × 100 m square transmitter loop and a central receiver, measuring the vertical component of the magnetic field.

The 1D TEM-MT joint inversion performed in this study was done using the TEMTD software. The first layer of the initial model was assigned a fixed thickness of 10 m and the half-space was given a constant resistivity value between 10 and 30 Ωm. For most of the inversions an initial model with 50 layers was used. Damping factors were applied to smoothen the output model. The misfit of the model was evaluated by the chi-square factor. The highest chi-square error in the final fit was 11.6, most errors were less than 2 (see Appendix II in Didas, 2018). The inversion was done by jointly inverting the TEM data and the rotationally invariant apparent resistivity and phase of the MT data calculated from the average (arithmetic mean) of the off-diagonal impedance tensor elements. The static shift multiplier was one of the parameters in the inversion. An example of a 1D MT/TEM joint inversion is shown in Figure 13.

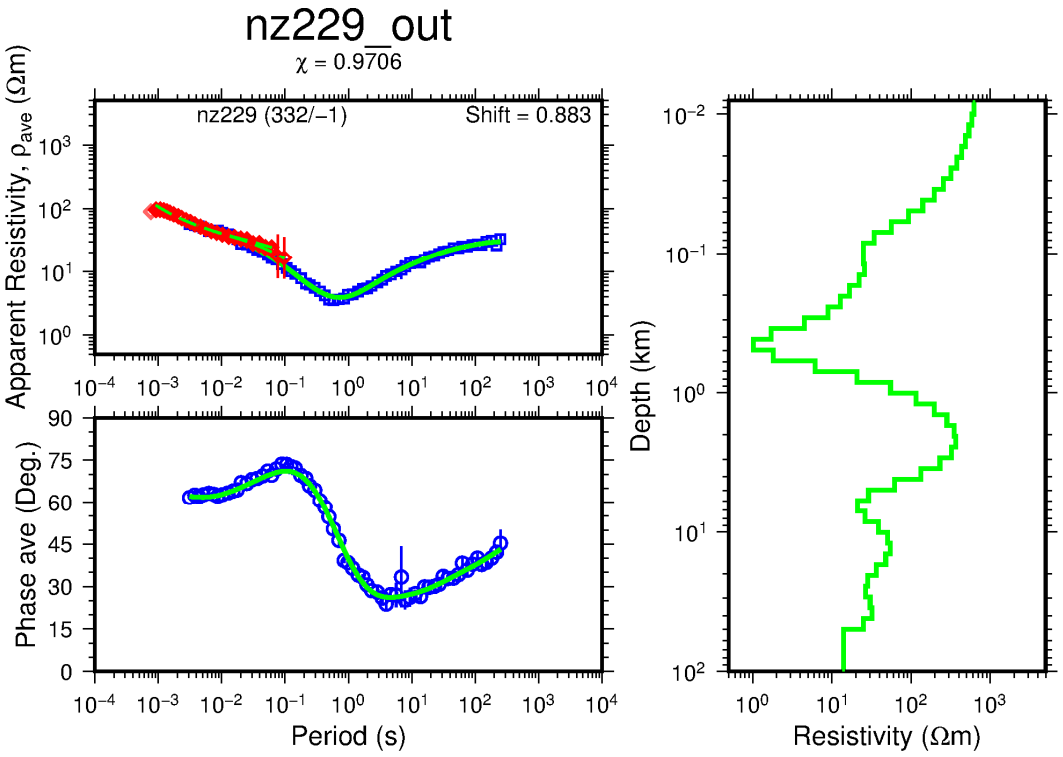

FIGURE 13: Example of the result of joint 1D Occam inversion of TEM and MT data. Red diamonds are measured TEM apparent resistivities, blue squares are measured MT apparent resistivities, and blue circles are the MT phase. The green curve to the right shows the Occam resistivity model vs. depth. The calculated response of the resistivity model is given by the solid green lines in the two panels to the left. The shift multiplier is shown in the upper right-hand corner of the apparent resistivity panel. The 322 m in the parentheses (x/y) are due to differences in coordinate projections between collocated MT (in WGS84) and TEM (in ARC1960) stations.

8.1 Static shift multiplier of MT data in Ngozi prospect

In the Ngozi prospect, the static shift multiplier for 64 MT soundings was calculated using arithmetic mean invariant values for the apparent resistivity through joint inversion with data from a nearby TEM sounding. The spatial distribution of the multipliers is shown in Figure 14. The multipliers were in the range of 0.1-4.7, most commonly around 0.6 (Figure 15). In the static shift correction of MT data, the apparent resistivity values are

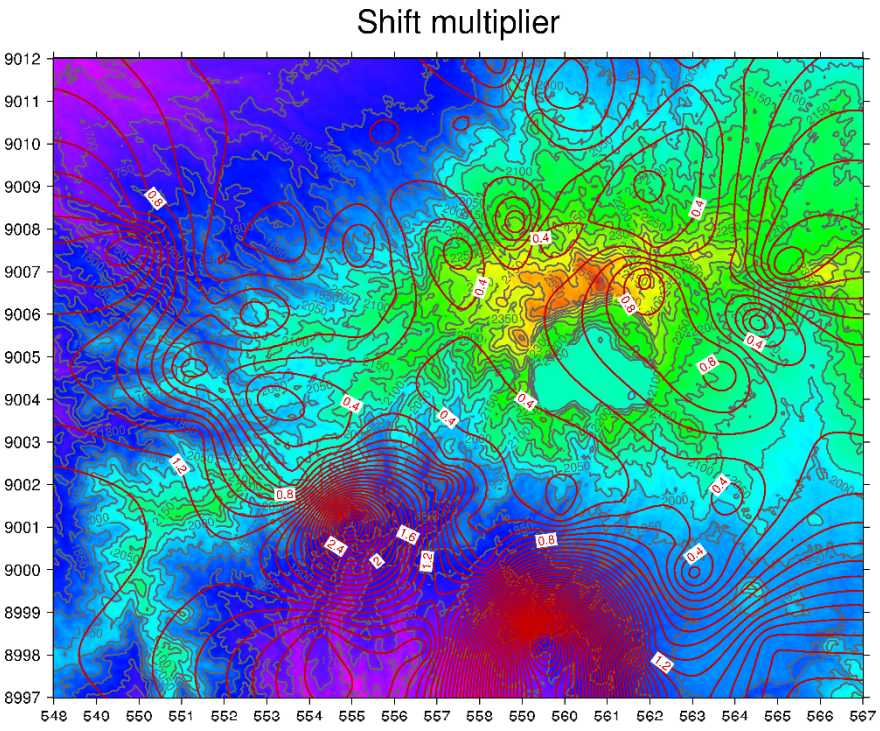

FIGURE 14: Spatial distribution of static shift multipliers in the Ngozi prospect

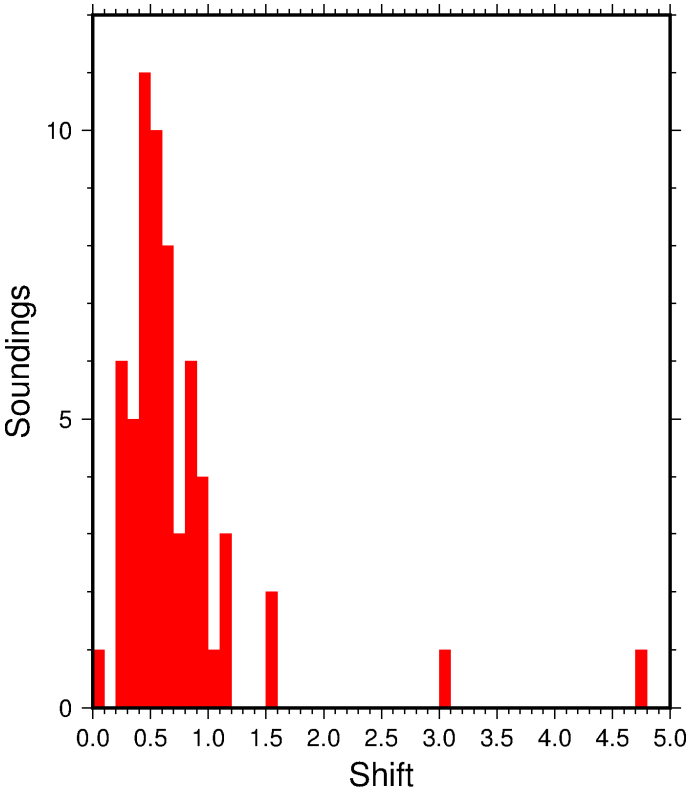

FIGURE 15: Histogram distribution of static shift multipliers in Ngozi prospect

divided by the shift multiplier. From the histogram (Figure 15) we can see that the majority of the soundings were shifted up (shift factor <1) and only a few shifted down (shift factor >1). The highest static shift factors are observed southwest and northwest of the Ngozi caldera where shallow-subsurface alluvial sediments are found. The low static shift factors are observed around the dome area at high topography where steep slopes are likely to have strong distortion effects on the telluric currents as discussed in Section 5.5.2.

9. RESULTS OF THE 1D JOINT INVERSION

The result of 1D Occam inversion of 64 co-located MT/TEM sounding pairs, using the arithmetic mean invariant values for the MT apparent resistivity and phase, are presented here in three ways; firstly as 1D model for each TEM/MT jointly inverted sounding pair (Appendix II in Didas, 2018), secondly as vertical resistivity cross-sections and thirdly as resistivity maps at different elevations (depth slices). Finally, the strike analysis and induction arrows are discussed.

9.1 Resistivity cross-sections

The resistivity cross-sections in this study were generated using the TEMCROSS program (Eysteinsson, 1998). All the resistivity cross-sections (compiled from the 1D models) are displayed in Appendix III in Didas (2018). They show resistivity structures to 5 km depth. Their locations are displayed in Figure 16 and five of them (Figures 17-21) are discussed in this report to emphasize the main results of the 1D inversion.

9.1.1 Resistivity cross-section along profile 5

The cross-section in Figure 17 is located about 2,400 m south of the Ngozi caldera lake. It trends from southwest to northeast and crosses the southwest dipping NW trending inferred thrust fault mapped by Alexander et al. (2016) at MT station nz248. The main visible features are:

a) A resistive surficial zone of 100-200 Ωm and maximum thickness of about 200 m.
b) A well-defined conductive cap of 1-10 Ωm with thickness of about 500 m, centred at a depth of about 1,400 m a.s.l.
c) A 10-30 Ωm conductive layer with thickness of up to 1 km, which surrounds the conductive cap.
d) A moderately resistive zone of 30-70 Ωm below the conductive layer with thickness of about 1,500 m centred at sea level.
e) A vertical conductive anomaly of 10-30 Ωm, 5 km wide with some very conductive < 10 Ωm patches below the moderately resistive zone imaged by MT stations ng00 and nz316.
f) A resistive zone of 70-100 Ωm to the east of the vertical conductive anomaly.

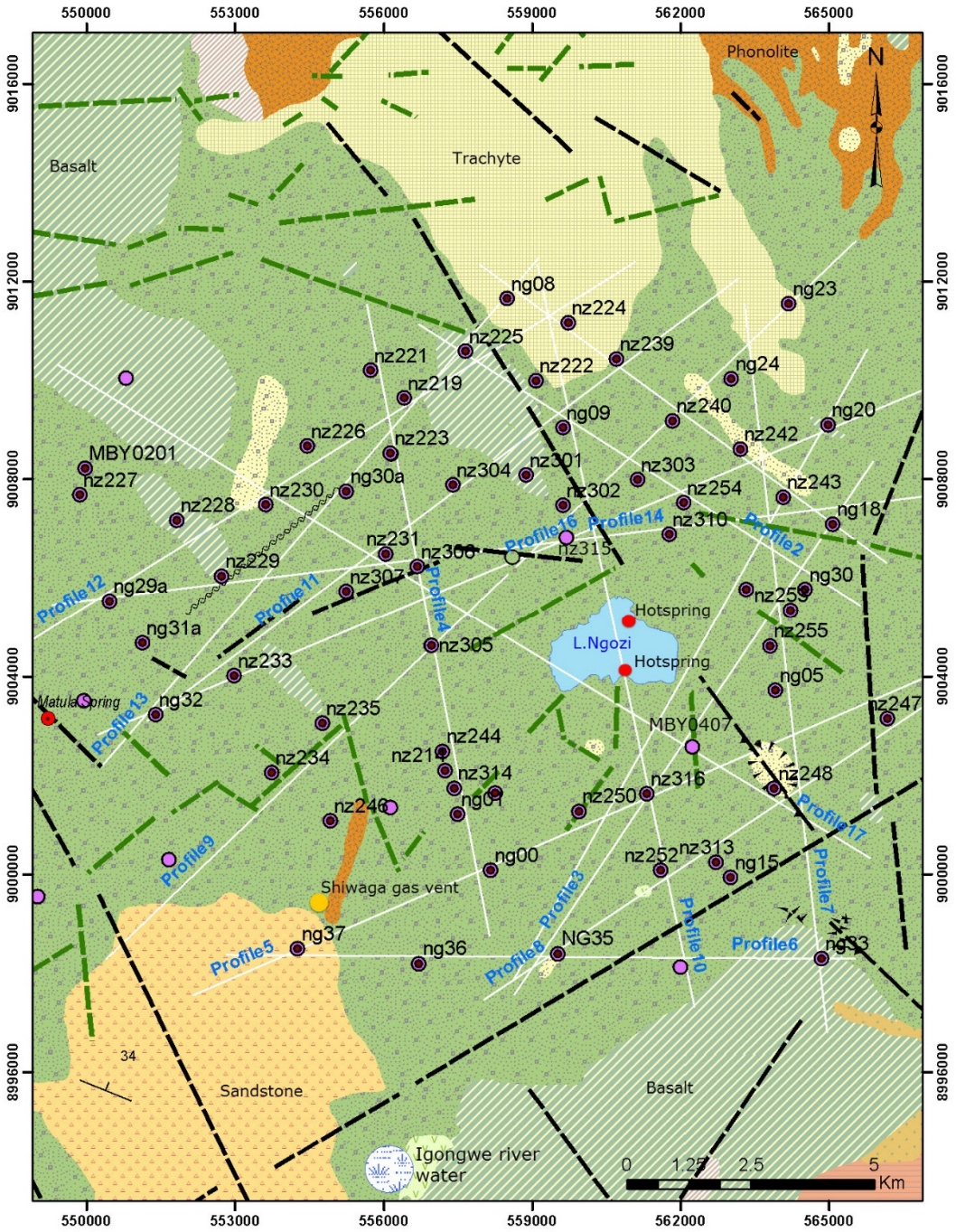

FIGURE 16: Location of the resistivity cross-sections (white lines superimposed on the Ngozi geological map). The black stippled lines are the inferred faults mapped on the surface and green lines are lineaments extracted from Shuttle Radar Topographic Mission 90 m resolution Digital Elevation Model. The black dotted circles are the MT/TEM sounding pairs and MT stations without TEM are circles without dots

g) A very resistive zone of 100-200 Ωm to the west of the vertical conductive anomaly. The top surface is defined by 100 Ωm iso-resistivity line below the Shiwaga CO_2 gas vent down to a depth of about 1,000 m.

9.1.2 Resistivity cross-section along profile 9

Cross-section along profile 9 (Figure 18) is located 1,800 m northwest of Ngozi caldera (see Figure 16).

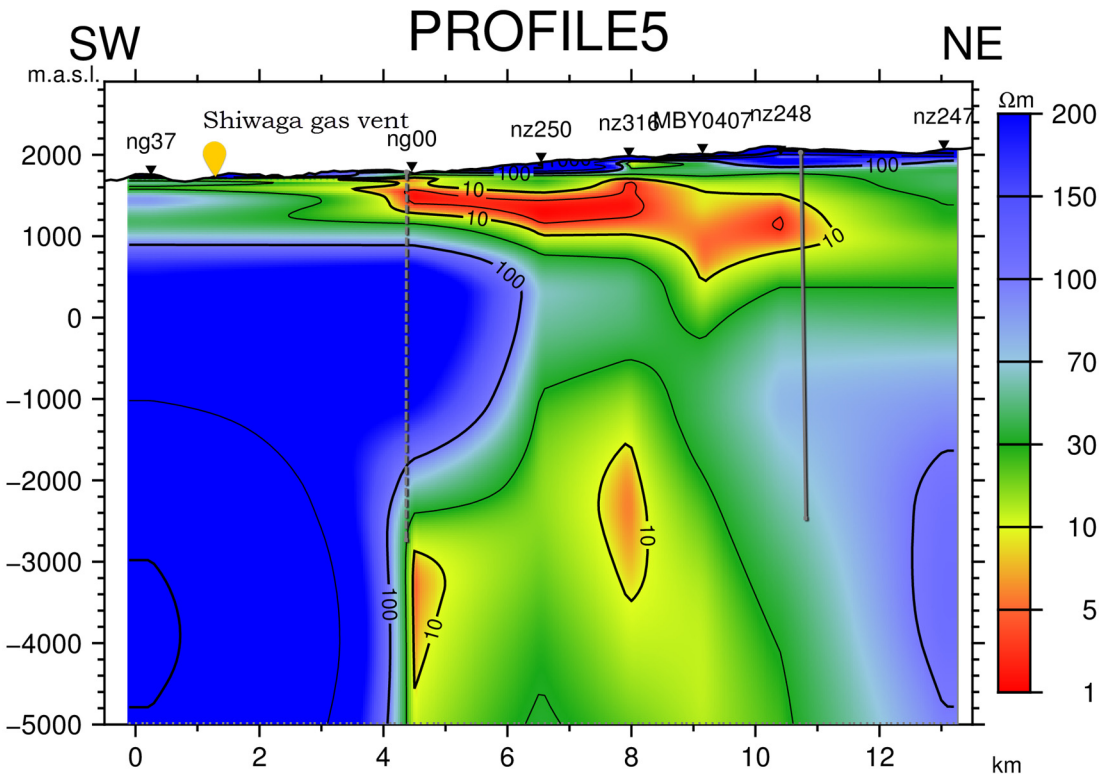

FIGURE 17: Resistivity cross-section along profile 5 (location on Figure 16); the grey straight line is the projection of the inferred fault mapped at the surface and the dotted line represents the western end of the same fault

The cross-section was generated with the purpose of observing the north extension of the fault zone revealed in profile 5 (Figure 17) which is located about 2,400 m south of the Ngozi caldera. The main observations are:

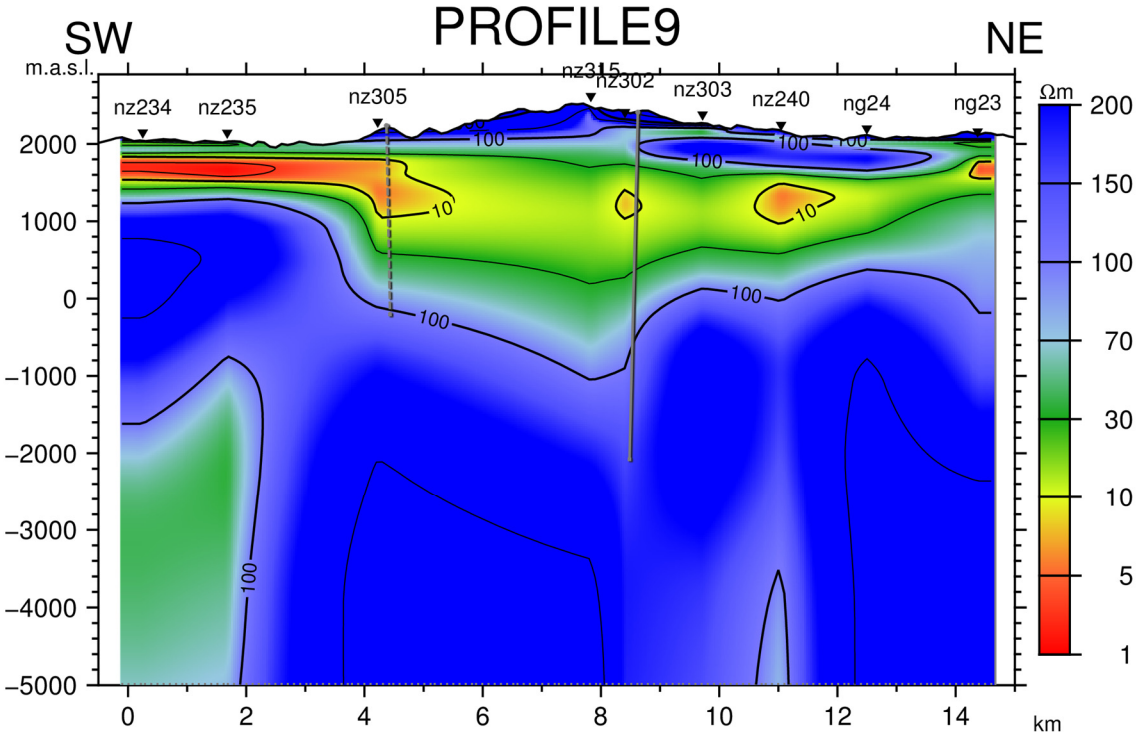

FIGURE 18: Resistivity cross-section along profile 9 (location on Figure 16)

a) The surficial resistive layer with resistivity > 100 Ωm thickening up to 500 m over the Ngozi caldera rim and thinning in south-westerly and north-easterly direction.
b) A 10-50 Ωm zone with some < 10 Ωm anomaly patches in the northeast. The layer is thickening within the fault zone between MT station nz305 and nz302 relative to the adjacent <10 Ωm resistivity anomaly in the southwest.
c) A well-defined 100 Ωm anomaly about 400 m thick below MT stations nz303, nz240 and ng24 below the resistive surficial layer.
d) A very extensive resistive zone with resistivity > 100 Ωm below the conductive anomalies from a depth of 1,200 m a.s.l. The top part is defined by the 100 Ωm resistivity iso-line.
e) A <100 Ωm resistivity anomaly imaged by MT stations nz234 and nz235 at a depth of about 1,500 m b.s.l.

9.1.3 Resistivity cross-section along profile 10

The cross-section along profile 10 (Figure 19) passes through the Ngozi hot springs located at the bottom of the lake and the NW-SE trending inferred fault at MT station nz302 (see Figure 16). The cross-section was generated with the purpose of mapping the southwest and northeast extension of the fault zone mapped north and south of the Ngozi caldera along profiles 5 (Figure 17) and 9 (Figure 18), respectively. The second purpose was to investigate the extension of a vertical conductive anomaly observed in cross-section 5 with MT station nz316 across the Ngozi caldera lake. Station nz316 is about 2,700 m to the south of the hot springs and station nz315 is about 1,600 m north of the lake. The main visible features are:

a) The resistive surficial zone with resistivity > 100 Ωm thickening towards the rims of Ngozi caldera lake and thinning to each side.
b) A moderately resistive zone (30-70 Ωm) (within the fault zone with sharp boundaries), overlain by the thick resistive surficial layer.
c) The conductive layer (< 10 Ωm), relatively horizontal to the south-southeast and north-northwest, respectively, terminates before reaching the Ngozi caldera. The conductive anomaly on top of the

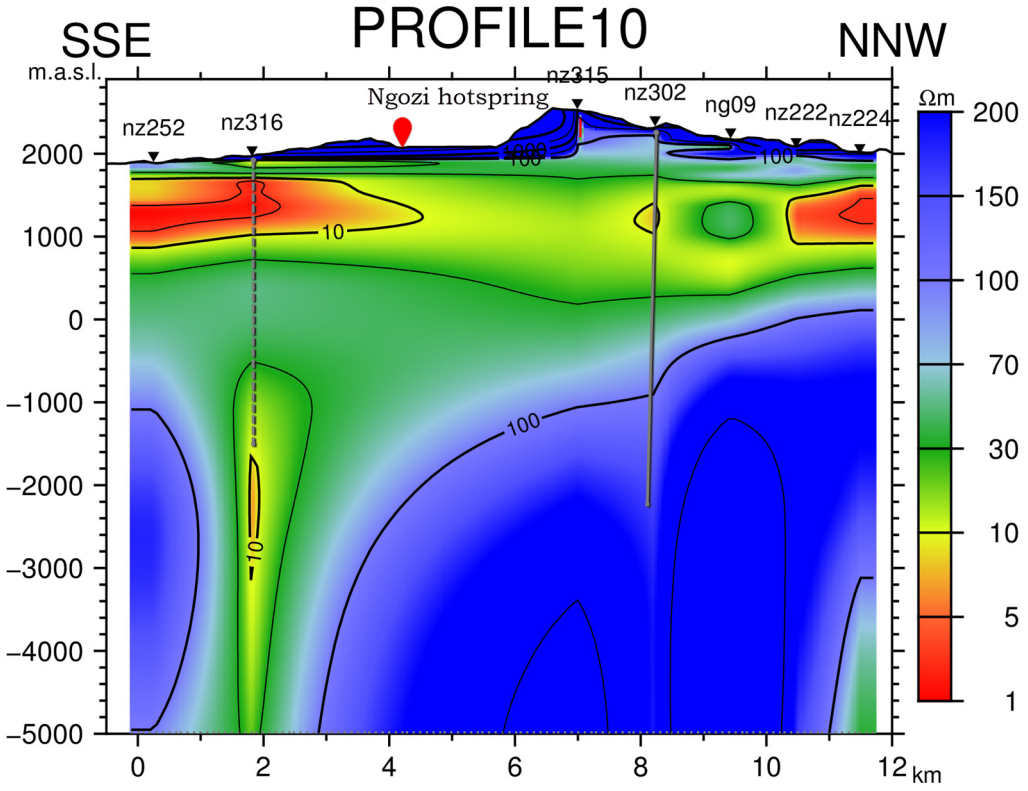

FIGURE 19: Resistivity cross-section along profile 10 (location on Figure 16)

vertical anomaly is elevating from nz252 to nz316 as it approaches the fault boundary south-southeast of the Ngozi hot spring. However, there is no MT station close to the lake to justify the exact thinning of this anomaly.

d) A vertical moderate conductive zone (> 10-30 Ωm) below MT station nz316 associated with a 10 Ωm patch.
e) The very extensive resistive zone of > 100 Ωm below the conductive anomalies from around sea level in the north-northwest part and down to 1,000 m b.s.l. in the south-southeast. The top part of this anomaly is defined by the 100 Ωm iso-resistivity line.

9.1.4 Resistivity cross-section along profile 11

Cross-section along profile 11 (Figure 20) is located about 3,700 m northwest of Ngozi caldera lake and about 1,900 m away from profile 9 (see Figure 16). The cross-section was generated with the objective to investigate the northern extension of the fault zone mapped in cross-section 9 (Figure 18). The main visible features are:

a) The resistive surficial layer (> 100 Ωm), thickening to about 600 m at the centre of the cross-section and thinning to both sides.
b) A conductive layer (< 10 Ωm) of about 200 m thickness southwest of the cross-section, thickening to about 800 m northeast of the cross-section. The northeast anomaly is enclosed by the 10-50 Ωm resistive anomaly. It is displaced downwards between MT station nz307 and nz231 to a depth of about 1,000 m by the fault mapped at the surface (Figure 16).
c) A 10-50 Ωm resistivity layer located below the conductive layer (< 10 Ωm) in the southwest and overlain by the resistive surficial layer from the central part of the profile towards the northeast. It is up to 2 km thick within the fault zone and elevated in southwest direction.
d) A vertical resistivity anomaly of 70 and 100 Ωm and 4 km wide below the fault zone.
e) A resistive (> 100 Ωm) extensive zone overlain by the 10-50 Ωm layer and separated by a vertical resistivity anomaly of 70 and 100 Ωm. Similarly, the top of these anomalous zones is defined by a 100 Ωm iso-resistivity line.

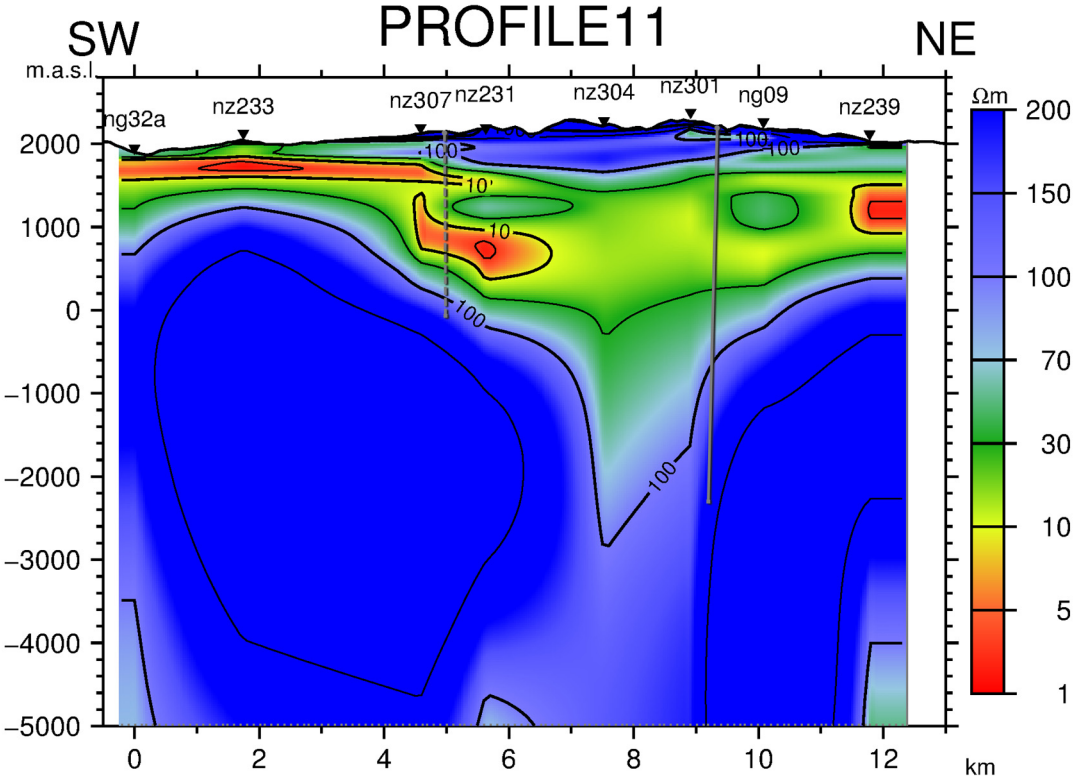

FIGURE 20: Resistivity cross-section along profile 11 (location on Figure 16)

9.1.5 Resistivity cross-section along Profile 12

The cross-section along profile 12 (Figure 21) is located 5,600 m northwest of Ngozi caldera lake (see Figure 16). It was made to trace further the extension of the fault mapped in profile 11, located about 1,800 m south, where the fault is observed to show little displacement in the resistivity anomalies. The main visible features are:

a) A thin surficial resistive layer (> 100 Ωm) thinning away from the centre.
b) A 100 Ωm anomaly about 100 m thick between MT station nz230 and nz225 below the resistive surficial layer.
c) The very extensive high conductive layer (< 10 Ωm) below the surficial resistive layer with thickness ranging from 400 m to 1,000 m. This layer is deep and thick at the centre of the cross-section and is more elevated towards the SW where it is covered by a thin resistive layer.
d) A thick resistive zone (> 100 Ωm), its top is defined by a 100 Ωm iso-resistivity line extending to great depth.
e) A 30 -70 Ωm resistivity anomaly at greater depth of about 4,000 m b.s.l. revealed below MT station nz224.

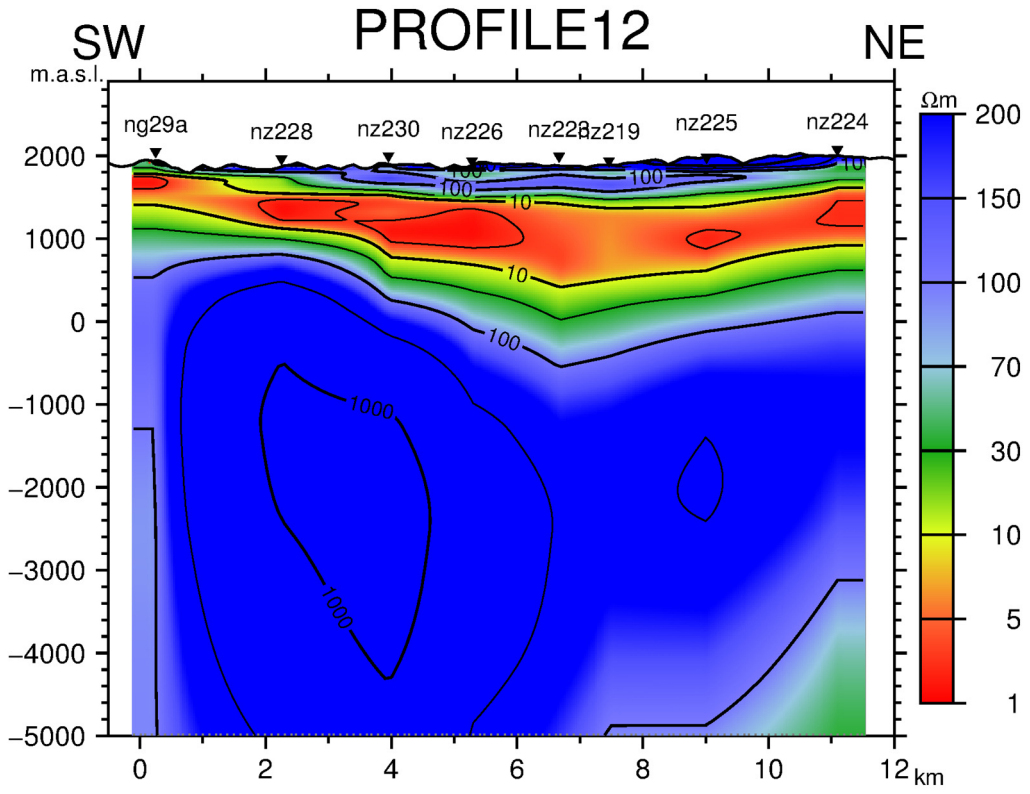

FIGURE 21: Resistivity cross-section along profile 12 (location on Figure 16)

9.2 Resistivity maps

Resistivity maps presented in this study were made with the TEMRES program (Eysteinsson, 1998). They were generated from the jointly inverted MT-TEM sounding data, through the 1D Occam models. The maps help to understand the general lateral trend of the resistivity distribution at different depths throughout the entire surveyed area of the Ngozi prospect. As indicated on the location map (Figure 16), there is a gap due to lack of MT-TEM stations close to Ngozi caldera because of limited accessibility. This gap poses a limitation to the understanding of the general trend of resistivity below the caldera where the high-temperature manifestations are found. Therefore, interpolating resistivity models around the caldera contain uncertainties. Here, three selected resistivity maps are discussed (at 1,500, 1,000 and

500 m a.s.l.) for interpretation purposes (see Figure 22-24). More maps can be found in Appendix III (Didas, 2018).

9.2.1 Resistivity map at 1,500 m a.s.l.

The map (Figure 22) was generated with the objective of showing the lateral extent of the conductive anomaly (< 10 Ωm) in the area. The anomaly is thought to present alluvial clay rich sediments deposited within the NW-SE trending paleo-basin. The main visible features are:

a) A conductive anomaly (< 10 Ωm) trending NW-SE west of Ngozi caldera. From south to north the anomaly is truncated by a > 10 Ωm anomaly.
b) A resistive anomaly (> 100 Ωm) incising east and southwest of the map which could be representing the low permeable rock which is less or not affected by geothermal alterations.

9.2.2 Resistivity map at 1,000 m a.s.l.

This map (Figure 23) was generated primarily to investigate the lateral extent of the base of the conductive (< 10 Ωm) anomaly and secondly to investigate the lateral extent of the top of the moderately resistive anomaly thought to be the top of the geothermal reservoir. These are the main visible features in the map:

a) Distinct very conductive (<10 Ωm) anomalies located south and north of the moderately resistive anomaly (10-50 Ωm), probably representing the bottom patches of the clay rich formations.
b) A well-defined NW-SE trending anomaly characterised by intermediate-resistivity values (10-50 Ωm) engulfing the Ngozi caldera lake, representing the top part of the reservoir.
c) Two anomalies of high-resistivity core (>100 Ωm) bounding the moderately resistive anomaly to the east and west, respectively, representing low permeability zones likely to be the basement.

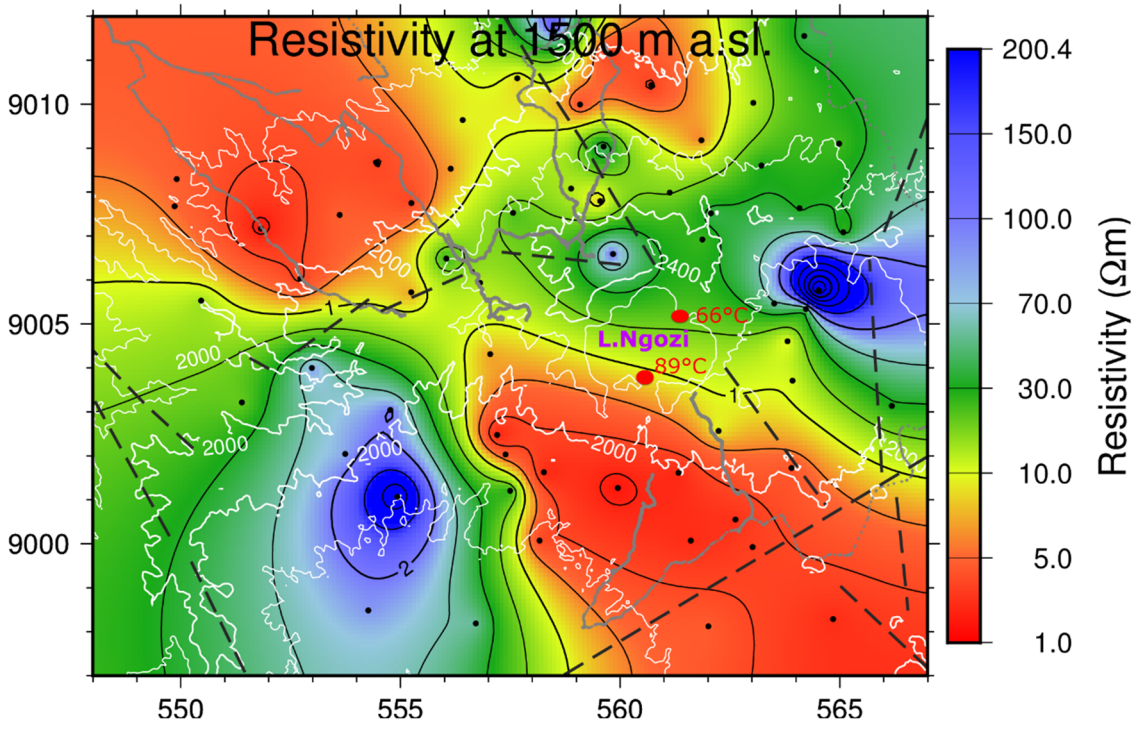

FIGURE 22: Map showing the lateral resistivity distribution at a depth of 1,500 m a.s.l. The grey lines are the accessible roads and field tracks and the black dotted lines are the inferred faults mapped on the surface. Black dots are MT stations and the red dots are the hot springs located at the bottom of Ngozi caldera lake, which is indicated by the circular contour line. The resistivity contours on the map are in logarithmic scale

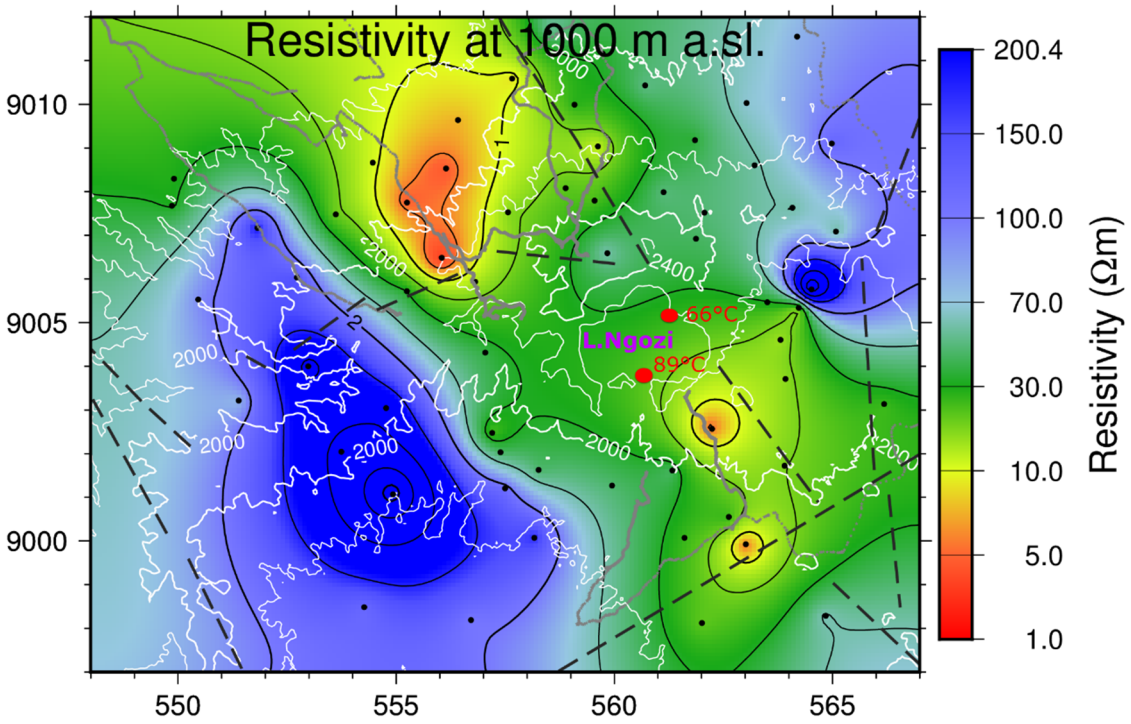

FIGURE 23: Map showing the lateral resistivity distribution at a depth of 1,000 m a.s.l. (see Figure 22 for legend)

9.2.3 Resistivity map at 500 m a.s.l.

A resistivity map at 500 m a.s.l. (Figure 24) was generated to investigate the lateral extent of the moderately resistive anomaly (30-70 Ωm) observed in most of the cross-sections, bound to the east by the inferred fault mapped at the surface (see Figure 16). The secondary objective was to investigate the western end of this fault. The visible features are:

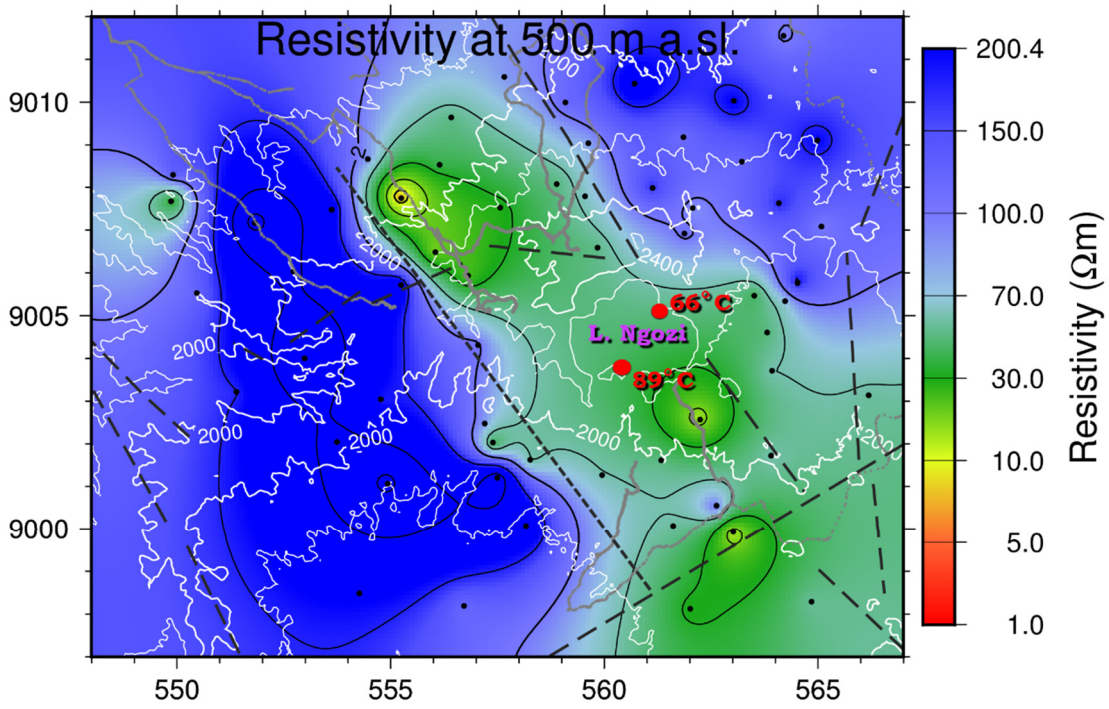

FIGURE 24: Map showing the lateral resistivity distribution at a depth of 500 m a.s.l.; the map cuts through the middle portion of a probable reservoir, hermetically closed within the fault zone

a) An intermediately conductive core (30-70 Ωm), clearly visible in the central part of the survey area and in good agreement with the NW-SE trending inferred fault zone mapped at the surface. Similarly, it engulfs the Ngozi caldera lake and extends further to north and south. Considering the presence of the hot springs in the Ngozi caldera, the fault zone is likely to be controlling the high-temperature geothermal system in the area as manifested by its low resistivity values relative to the surrounding area. The low resistivity within the fault zone is an indication of a hermetically closed high-permeability zone which could be an important production zone.
b) The eastern and western part of this anomaly (the low resistivity within the fault zone) is dominated by a high-resistivity core with resistivity value of > 100 Ωm, which is in agreement with the low-permeability metamorphic basement.

9.3 Strike and induction arrows analysis

The geoelectrical strike direction (Figures 25 and 26) gives information about the 2D resistivity structure, that is in which direction the resistivity changes the least. As discussed earlier, in a 2D earth model the resistivity varies with depth and in one of the two principal horizontal directions. The strike direction is represented by the induction arrows or strike rose diagrams generated from the vertical magnetic field Hz, i.e. Tipper tensor for each MT station. Since the Tipper is a complex vector, it can simply be represented by two induction arrows, one containing the real part, the other the imaginary part. Usually, only the real induction arrows are used. According to Parkinson convention (Parkinson, 1959; Berdichevsky and Dmitriev, 2002), the imaginary part is sensitive to resistivity contrasts close to the measurement site while the real part is more sensitive to regional resistivity contrasts. As described by Parkinson (1959), the real induction arrows point towards regions characterized by current concentration, i.e., high conductivity and away from zones of low conductivity. The imaginary part is normally pointing away from a zone of high conductivity towards a zone of high resistivity. The size of

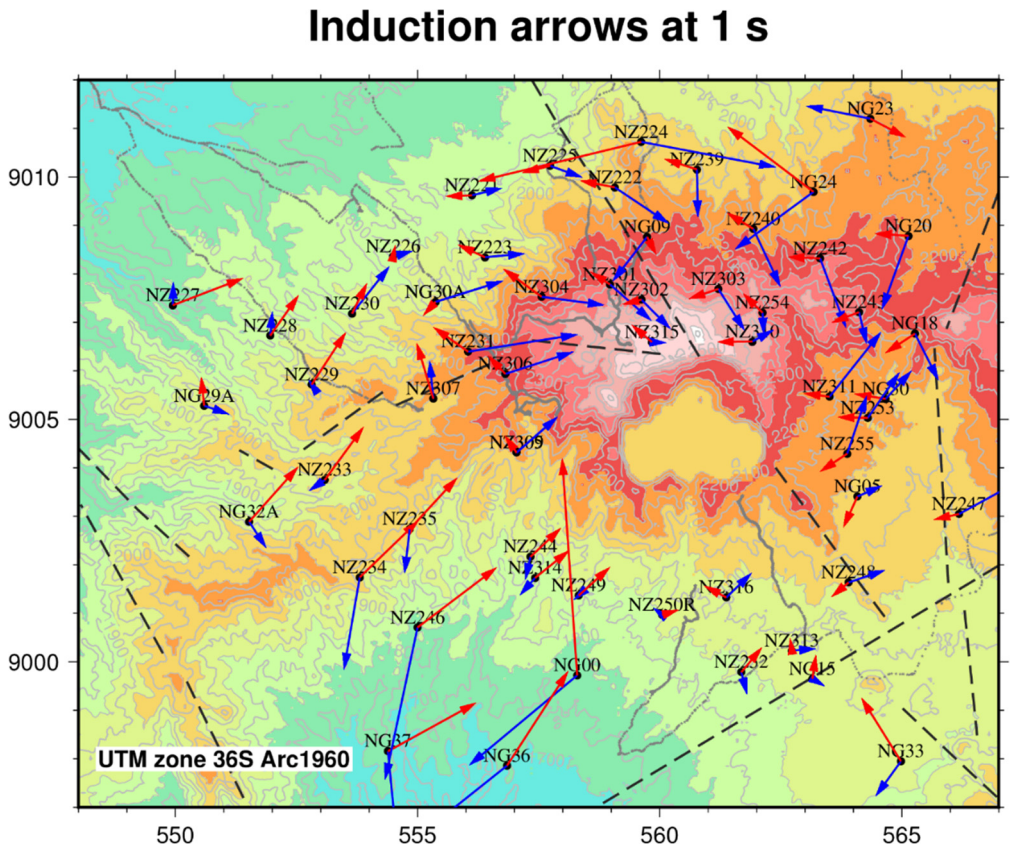

FIGURE 25: Induction arrows for the period of 1 s; the blue arrows are the real part and the red arrows are the imaginary part; figure legend as shown in Figure 22

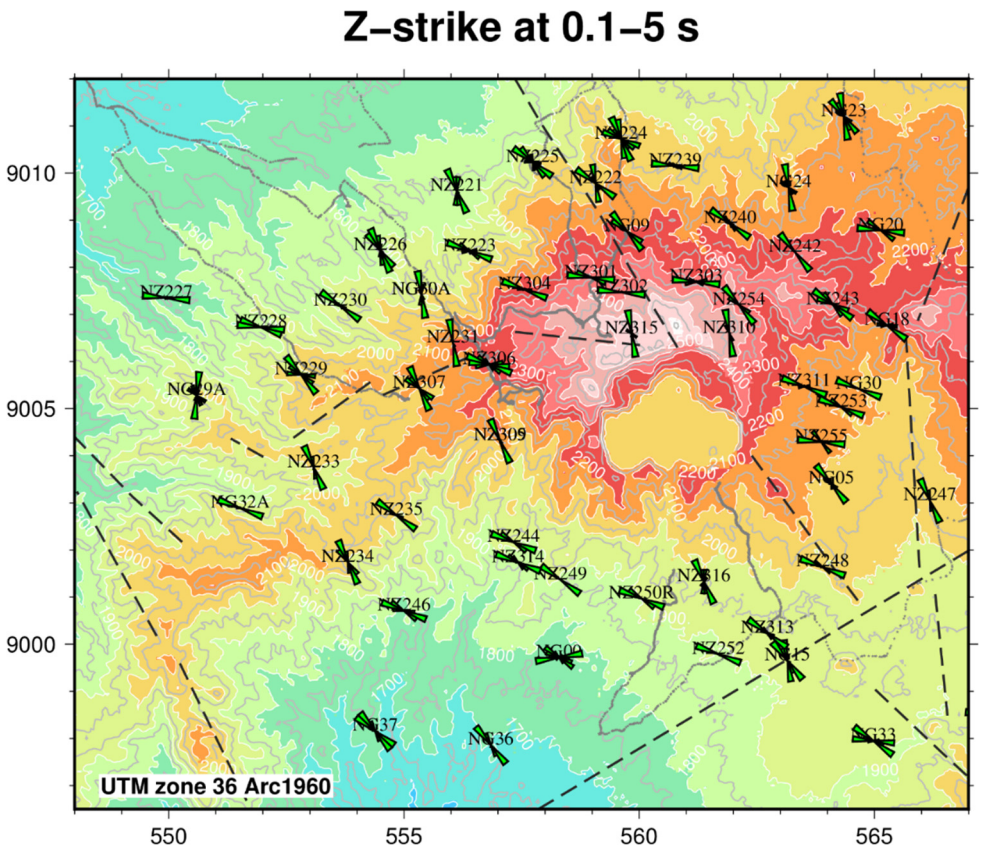

FIGURE 26: Zstrike for the period of 0.1-5 s; Figure legend as shown in Figure 22

the arrows depends on the magnitude of the vertical magnetic field. If the magnitude of the vertical magnetic field is small the induction arrows will be small and vice versa.

For a 2D earth, the real and imaginary arrows are co-linear and point perpendicular to the strike of the 2D geoelectrical structure (Berdichevsky and Dmitriev, 2002). However, asymmetry of the medium violates the co-linearity of the real and imaginary parts and thus, the real and imaginary part point in different directions. The direction perpendicular to the one of the imaginary and real part is called the geoelectric strike (Hersir et al., 2015b). The angle which the geoelectric strike makes with the geographical north is called Swift-angle or Zstrike. The Zstrike direction is found by minimizing the diagonal elements of the impedance tensor or by maximizing the off-diagonal ones. The shortcoming of this method is that there is a 90º ambiguity in the geoelectric strike. This problem is resolved by measuring the vertical magnetic field, Hz, which is generated by lateral conductivity gradients, and calculating the Tipper tensor/vector (Hz=TxHx+TyHy) (see Schmucker, 1970) which relates the vertical component of the magnetic field to its horizontal components and the strike is obtained by minimizing |Tx| (Vozoff, 1991). Tx and Ty are the x and y-components of the Tipper vector, respectively. 1D resistivity structures are devoid of excess currents. Hence, the vertical magnetic field component and the Tipper vector are zero, whereas Hz can be induced in 2D and 3D cases due to excess currents caused by horizontal variations in the electric currents (Berdichevsky and Dmitriev, 2002).

The electrical strike direction gives valuable information on subsurface fractures and permeability, not visible at the surface which are an important additional information for confirming the model, developing the conceptual model and siting of wells. The strike is a function of frequency and thus, changes with depth.

In this study the geoelectric strike analysis (Figures 25 and 26) of MT data was performed to investigate potential permeable zones which could help to revise the existing conceptual model. To make this viable,

multi-frequency plots of the strike and induction arrows inferring different depths for each MT sounding are plotted on a map (Figure 25). For clarity two maps are presented in this section but more maps can be viewed in Appendix IV in this study (Didas, 2018).

From the strike analysis shown in Figure 25, it can be observed that for a period of 1 s, the real induction arrows point towards the more conductive zone close to the Ngozi caldera. Using the Zstrike (Figure 26) the main electric strike is found to be northwest for most of the Ngozi MT stations. This trend is parallel to the fault zone mapped in this study (Figure 24) and can also be observed in the geological map of the area (Figure 16).

9.4 Geothermal interpretation of the results

A geothermal system consists of convection of water in the upper crust of the earth in a confined space and there it transfers heat from the heat source (e.g. shallow magma chamber or hot intrusive bodies) to the heat sink, usually the free surface. Thus, a geothermal system is made up of three main elements: heat source, a reservoir and fluid which is the carrier that transfers the heat. The geothermal reservoir is normally separated from the uppermost rocks by an impermeable relatively thick rock layer composed of smectite clay minerals as a result of geothermal fluid-rock interaction. In resistivity surveys, particularly MT, the elements of the geothermal system can be observed. The clay cap is normally very conductive, the reservoir is moderately resistive and the heat source (if present) below the reservoir is conductive. The rocks (cold rocks) not affected by geothermal processes normally give the highest resistivity signatures.

The high-temperature geothermal field in the Ngozi area is characterized by the following resistivity structures. Near the surface, it is characterized by the high-resistivity unit (> 100 Ωm) overlying a conductive cap which overlies a resistive core. Linking these units to the geology of the area, the high-resistivity unit near the surface is the ash-pumice (with thickness reaching over 1 km) with low or no alteration. The prominent highly resistive bodies whose top parts are defined by the 100 Ωm iso-resistivity line and extend to greater depths are interpreted as the low-permeability metamorphic basement.

The conductive layer (< 10 Ωm) in cross-section 5 (Figure 17) is the clay cap. The moderately resistive zone of 30-70 Ωm below the conductive layer with thickness of about 1,500 m centred at 500 m a.s.l. could be the geothermal reservoir with high-temperature clay minerals like epidote, chlorite and amphibole formed at a temperature greater than 230°C. A localized possible heat source is observed as very conductive patches (< 10 Ωm) within a vertical conductive anomaly of 10-30 Ωm (5 km wide) imaged below MT stations ng00 and nz316 in cross-section 5 (Figure 17). These are probably hot intrusives within the fault zone which are fed by a magma chamber located several kilometres below the reservoir. A similar signature is anticipated below the Ngozi caldera where the indicative high-temperature hot springs discharge at the bottom of the lake. However, there is no MT sounding to constrain this assumption.

The upper part of the intermediate resistive anomaly of 30-70 Ωm below the surficial resistive layer within the fault zone is likely to be a poorly developed clay cap of the geothermal system possibly composed of smectite-illite, formed at a temperature between 50 and 200°C. It is difficult to set a clear boundary between the clay cap and the reservoir except in profile 5 (Figure 17). The shallow-subsurface conductive horizontal anomaly located east, west and far north of the fault zone and the Ngozi caldera is interpreted as clay rich sediments which were deposited within the NW-SE trending paleo-basin (see Figure 22) with a considerable amount of conductive minerals of sedimentary origin or partly formed by alteration, like kaolinite, smectite and zeolite that have a high CEC. It is likely that the sediments might also be affected by geothermal alteration but this would be an ancient outflow, active before the development of the Ngozi caldera. It is also likely that, after the development of the caldera the geothermal system became hermetically isolated within the fault zone identified in this study. The

eastern flank of the identified fault zone was mapped during a geological mapping campaign by Alexander et al. (2016) but the western arm has never been mapped except in this study.

10. INTEGRATED INTERPRETATION OF THE RESULTS

Integrated interpretation means to attach the geological and geochemical labels (realities) from the previous studies to the MT results in this study to get a better understanding of the geothermal system of the area. The aim is to constrain their relationships, update the conceptual model, define the high priority area and propose exploration drilling targets.

10.1 The cap rock, reservoir and heat source

- The resistive surface layer (see the resistivity cross-sections) can be correlated with the layer of ash-pumice which is covering large parts of the prospect (see Figures 3 and 16). The underlying conductive layer within the fault zone correlates to the poorly developed smectite-illite clay cap formed at a temperature between 100 and 230°C in the geothermal system. The smectite-illite clay cap does not extend further east than MT station nz248 located close to the escarpment of the inferred thrust fault dipping southwest (see Figure 17). Similarly, the vertical conductive anomaly zone revealed by MT stations nz250, nz316, MBY407 and nz248 almost terminates at station nz248 where the mapped fault's escarpment is located.
- The base of the clay cap directly above the fault zone (possibly hosting the heat source) is elevated (up-doming) due to a tendency of smectite to transform to the more resistive illite and chlorite, clays characteristic for permeable reservoirs (see Figure 17). A similar phenomenon is described by Anderson et al. (2000) and Cumming and Mackie (2010).
- The imaged fault zone, if active, is likely to allow heat flow from the shallow heat source to the high-temperature reservoir (> 230°C) above and the occurrence of the concealed hot springs at the bottom of the Ngozi crater lake indicate subsurface geothermal activity within the fault zone (see Figure 24). Fracture permeability, mainly within the fault zone, controls the fluid flow. The locally elevated clay-cap just west of the conductive fault zone and east of the Shiwaga gas vent observed in cross-section 5 (see Figure 17) could be attributed to cooler inflow from west thus, resulting in a local increase in resistivity at the base of the clay cap. A similar phenomenon is described by Cumming (2009), and Cumming and Mackie (2010). As reported by de Moor et al. (2012), the CO_2 and He gases from Shiwaga gas vent originate from the mantle. Therefore, we preclude the link to the geothermal system observed east of the gas vent along profile 5 of this study.
- It is likely that the conductive fault zone imaged by MT station nz316 in cross-section 10 (see Figure 19) is the same fault which extends further towards the Ngozi hot springs and is expressed as a lineament in remote sensing data (see Figure 16). It is also evident north of the Ngozi caldera lake along cross-sections 9 and 11 (see Figure 18 and 20).
- The presence of the two extensive border faults to the east and west of the Ngozi caldera (2.5 km long, 1.6 km wide and 74 m deep) would prevent significant leakage of fluid from the high-temperature reservoir away from the fault zone. Only where the clay cap is fractured by faulting for example at the bottom of the Ngozi caldera lake, fluids can escape. The reservoir is hydrologically sealed off from the surrounding rocks (see Figure 24).
- The Shiwaga gas vent located at the phonolite and sandstone interfaces indicates a deep fault separating the two formations, and possibly a special constrained conduit which transported magma that cooled and formed phonolite. It is likely that the fault is associated with the extensive, NW-SE trending Mbeya front range fault (a fault associated with the Matula spring) located 3 km west of the geothermal system. And it is likely to be an important, concealed connection to the Shiwaga gas vent which is located to the northwest of it (see Figure 16). This fault, if extrapolated further south, will pass through the Shiwaga gas vent.

- The contact between the old volcanic rocks and the metamorphic basement is marked by the 100 Ωm iso-resistivity line. In general, the metamorphic rocks in the area are resistive and this indicates that they are impermeable and not much affected by geothermal alteration processes except within the fault zone (see Figure 24).
- The absence of up-doming of the clay cap close to the Ngozi caldera could be attributed to its destruction caused by collapse during the caldera formation.
- The adjacent conductive zones of clay rich sediments which are partly truncated by faulting could also be affected by an outflow. This could extend laterally for some distance and date prior to the formation of the caldera. A contemporaneous event could be the hydrologic sealing off the geothermal system within the zone of opposite dipping fault boundaries trending NW-SE.
- The absence of a conductive cap within the fault zone close to the Ngozi caldera could be attributed to two possible causes:
  - The first possible explanation is the absence of the clay rich sediments which could have been deleted during volcanic eruption phases from the Ngozi volcanic centre, contemporaneously with the development of the geothermal system. These sediments were occupied by trachyte volcanic rocks which have low magnesium content. These rocks were subject to geothermal heating and alteration and formed a mixed-layer clay cap composed of smectite-illite-chlorite which normally is not very conductive.
  - Another possibility is that the smectite clay was buried and heated at greater depth and eventually converted into a mixed-layer clay composed of smectite-illite, hence the increase in resistivity.
- The vertical, conductive anomaly imaged in cross-section 5 (see Figure 17) is an important signature indicating a possible heat source located at a depth between 4 and 5 km within the fault zone. The conductive patches in the vertical conductive zone could be young (< 1 ka), hot intrusives associated with the formation of the caldera, conductively supplying heat to the fault zone. However, a 3D inversion model is needed to test for quality and imaging uncertainty at greater depths. This is because most of the data in the area have 3D effects at greater depths. However, correlating the averages from the resistivity as proposed by Park and Livelybrook (1989), all four MT stations that imaged the vertical anomaly show the same value. Hence it should be sufficient to use a 1D model around this anomaly (see Appendix II in Didas, 2018).
- The conductive anomalies located east of the inferred fault could be a fossil geothermal system (or a series of small systems). This might possibly be peripheral outflow of the Ngozi geothermal system before it was hermetically isolated and enclosed within the fault zone as it is observed in this study. This is supported by promising geochemical evidence of a > 230°C hot upflow at the bottom of Ngozi caldera lake.
- The thick volcanic ash-pumice reaching a thickness of more than 500 m within the fault zone might be masking geothermal surface manifestations with the exception of the Ngozi caldera lake where the clay cap is likely to be intensely fractured due to the faulting.
- The conclusion drawn by this study is that the base of the argillically-altered volcanic rock formation overlies the Proterozoic metamorphic basement complex uncomformably, except within the fault zone which corresponds to the upflow zone (observed below Ngozi caldera lake). Similarly, the alluvial sediments overly either older volcanic rocks or the metamorphic basement in low elevated areas.
- Whether faults mapped on surface are divergent or conservative remains unclear since no movement has been observed on these faults. With the area being filled with thick deposits of pyroclastic material forming unconsolidated ash-pumice, it is difficult to trace this on the surface. Hence, most of the faults in the area are inferred, based on mapped lineaments. On the other hand, the resistivity results from this study show good correlations with the inferred geological structures. Whenever there is displacement of the shallow conductive anomalies in MT cross-sections, the geologists were able to map either an inferred fault, a shear zone or a lineament at the surface. Examples of these correlations are observed at profiles 2, 3, 4, 5, 8, 9, 10, 11, 13, 14, 15, 16 and 17 (see Appendix III in Didas, 2018).

10.2 Areal extent of the reservoir

The northeast limit of the reservoir (Figure 27) clearly coincides with the extensive (> 20 km long) NW-SE trending inferred thrust fault mapped at the surface during the geological survey by Alexander et al. (2016). This fault zone connects the Ngozi Rungwe and Kiejo main volcanic centres, interrupted by the NE-SW striking right lateral strike-slip fault. The north-western limit of this fault was not mapped at the surface during geological mapping campaigns but is clearly identified in the MT resistivity anomaly in cross-sections 5 and 9 (Figure 17 and 18) located about 2 km south and north, respectively, of the Ngozi caldera lake. The width of this fault ranges from 4 to 7 km. In this study, the north-eastern limit of the fault zone mapped at the surface is indicated by the dislocation of the smectite clay-cap with significant downward movement at MT station nz305 while its north-eastern limit lies at the inferred fault at MT station nz302. The lateral distance between MT stations nz305 and nz302 is about 4 km, similar to the distance mapped in the south of Ngozi caldera in cross-section 5 between MT stations ng00 and nz248.

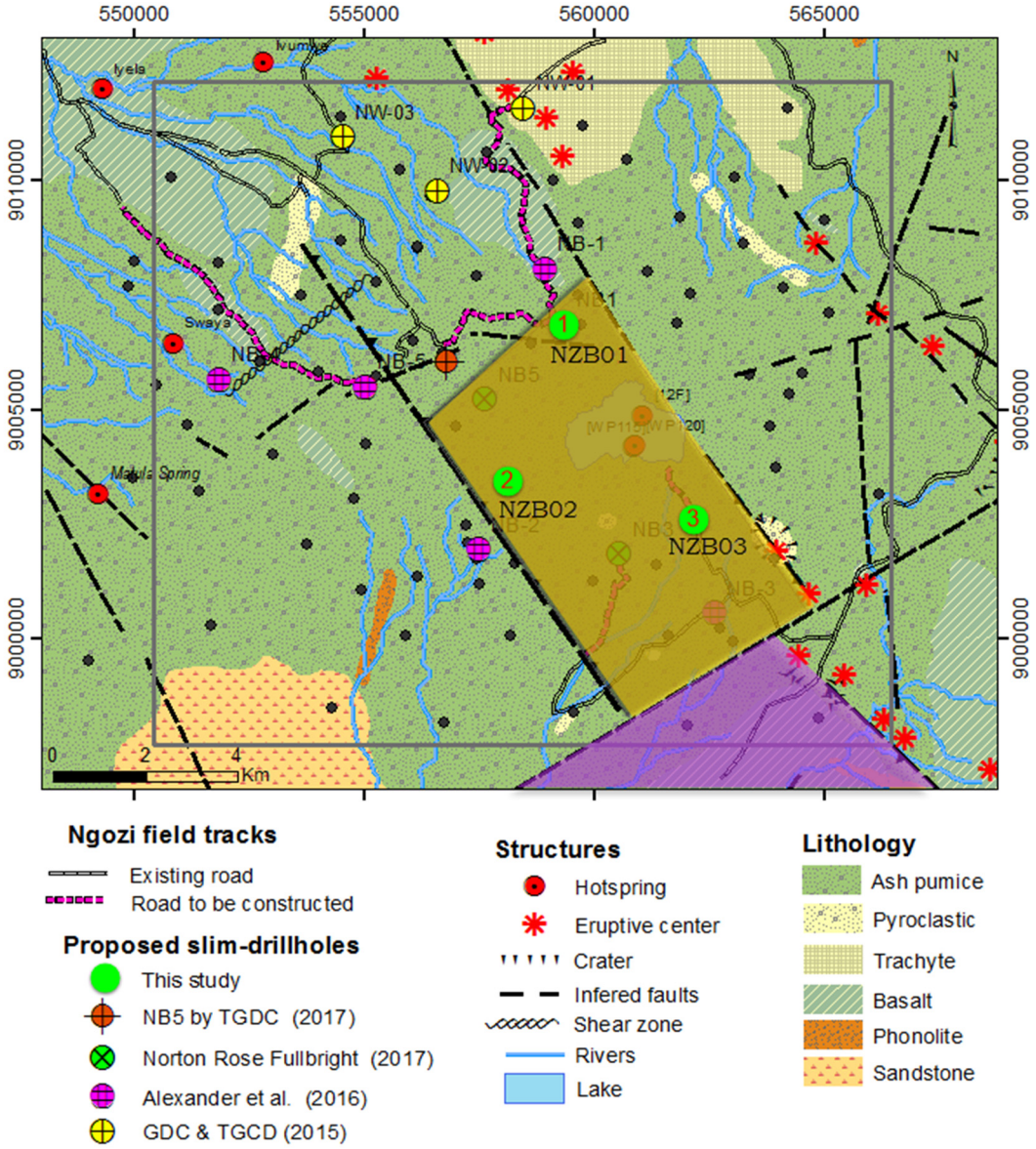

FIGURE 27: Areal extent of the geothermal reservoir; the first priority zone is the orange zone (zone in the middle bound by faults); the magenta coloured zone is the second priority zone (lower right corner); the numbered green circles are the drilling sites proposed in this study; while the black dots are the MT-TEM stations

The fault zone has small deformations from its linear direction, beyond cross-section 9 (Figure 19) as observed in cross-section 11 (Figure 20) and does not extend through profile 12 (Figure 21). Here, the shallow conductive layer might be associated with clay rich sediments deposited in the rift. Considering the observations mentioned above, the northeast and northwest extension limits of the reservoir are assumed to be within the fault zone, with a maximum width of 4 km wide and length of 7 km, as shown in Figure 27.

The estimated geothermal areal extent is related to the area´s fracture permeability assuming that the fluids ascending along the fault zone spread laterally more to northwest and do not escape from the fault zone either to the east or west. Thus, the geothermal system is hydrologically closed off, with the mapped NW-SE trending inferred thrust fault acting as the major barrier to the east and its western concealed boundary. This observation is supported by the absence of chlorine water escaping from the reservoir hosted in the fault zone and manifested by the hot springs below the Ngozi caldera lake. Thus, as pointed out in the geochemical section of Alexander et al. (2016), the hot springs located west of the identified fault zone are heated by conductively heated basement rocks and no NaCl rich waters from the high-temperature geothermal reservoir located below the Ngozi caldera are mixed in. By adopting the above mentioned landmarks, the zone of first priority, as represented in Figure 26, has an areal extent of 28 km^2.

10.2.1 Top of the reservoir

The depth down to the top of the reservoir is estimated based on the results of the 1D resistivity model shown in cross-sections in Figures 17-19, assuming the iso-resistivity line of 70 Ωm as the contact between the cap rock and reservoir. The top of the reservoir is at a depth of 1,000 m b.g.l. with the tendency to deepen towards the Ngozi caldera reaching a depth of 1,500 m b.g.l. north of the caldera. This is likely to be a consequence of the collapse during the Ngozi caldera formation as indicated in the cross-section in Figure 18.

10.2.2 Bottom of the reservoir

The bottom of the reservoir is not resolved in most of the cross-sections except along profile 5 (Figure 17). Here, the bottom of the reservoir is assumed to correlate with the iso-resistivity line of 30 Ωm above the vertical conductive anomaly within the fault zone interpreted as the heat source by this study. Thus, the bottom of the reservoir is assumed to be at the depth of -600 m b.s.l.

10.2.3 Vertical extent of the reservoir

Similar to the information obtained in the MT survey on the top and the bottom of the reservoir, as described above, the thickness of the reservoir is estimated to be of the order of 1,000 to 1,500 m.

10.3 Evidence for water mixing in the reservoir from geochemical results

A significant mixing of geothermal water with near surface water is reported for Igogwe river which is located about 11 km southwest of the Ngozi caldera lake (Kraml et al., 2008; Josephat, 2016). However, the mixing pathway was not unveiled and is explained here for the first time. The geochemical analysis of the Igogwe river water sample taken at location 33.5124º longitude and -9.10107º latitude (see Figure 16), shows a concentration of 252 mg/l (Josephat, 2016; Kraml et al., 2008). This significant amount of chlorine was interpreted to be the result of mixing with the water from Lake Ngozi which is the only known chlorine water source in the area. The sampling location lies along the NE-SW fault zone which transects the NW-SE fault zone (mapped in this study) hosting the geothermal reservoir (see Figures 16 and 26). Thus, a limited amount of geothermal water might be leaking through this fault and being discharged into the Igogwe River. The geochemical analysis of the adjacent Matula and Shongo hot springs located in the west and Swaya, Mwasanga and Iyela hot springs in the northwest, shows no

evidence of mixing with either the water from Ngozi crater lake or from the high-temperature geothermal reservoir (Kraml et al., 2008; Alexander et al., 2016; Josephat, 2017). This observation reinforces the believe that the geothermal system is hydrologically closed off within the fault zone as observed here. Furthermore, it is likely that faults with significant permeability tapping the geothermal water from the fault zone are lacking. Thus, this observation needs to be considered when locating recharge wells.

11. A REVISED GEOTHERMAL CONCEPTUAL MODEL AND DRILLING TARGETS

An integrated conceptual model of the Ngozi geothermal system (Figure 28) is developed in this study with the aim to target sites for possible exploration wells. The geothermal system is sealed within the convective fault zone.

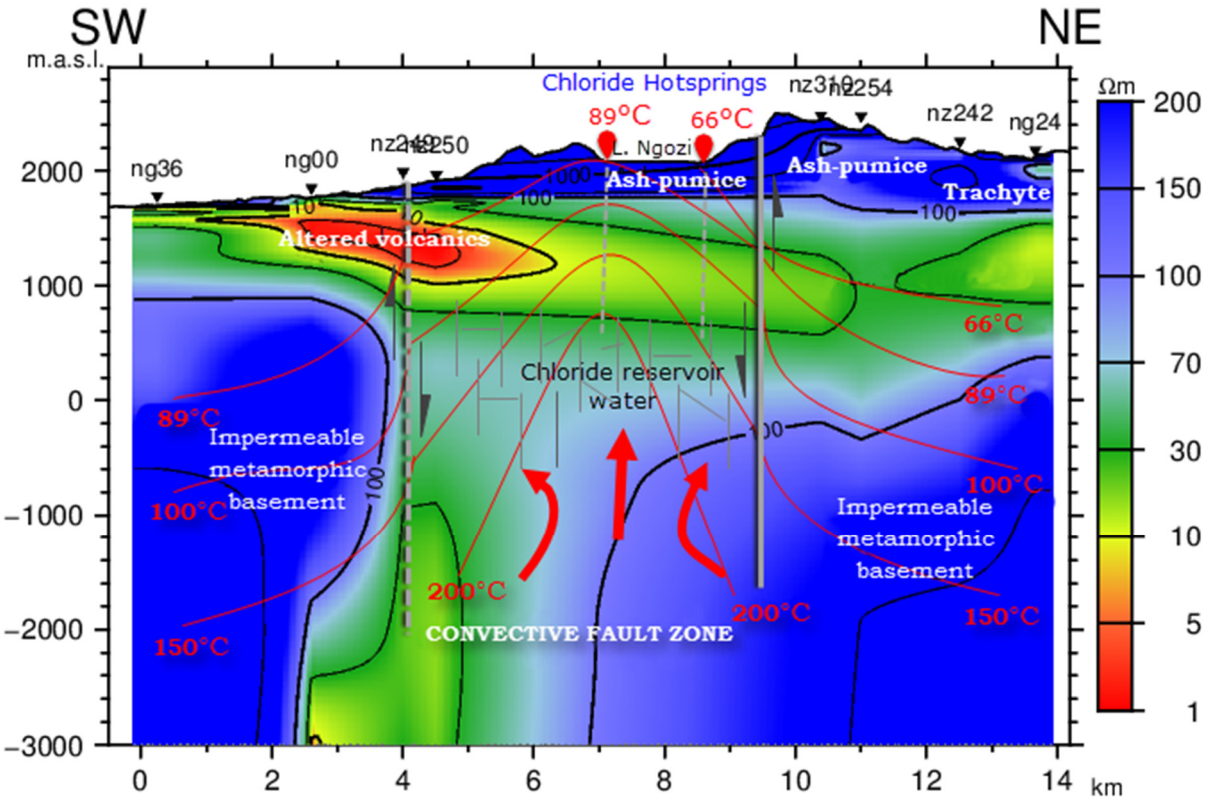

FIGURE 28: A revised geothermal conceptual model of the Ngozi prospect; the grey line is the mapped fault and the dotted line represents the extension of the same fault observed in this study. The curved lines are isothermal lines and the thick arrows indicate the heat flow within the fault zone

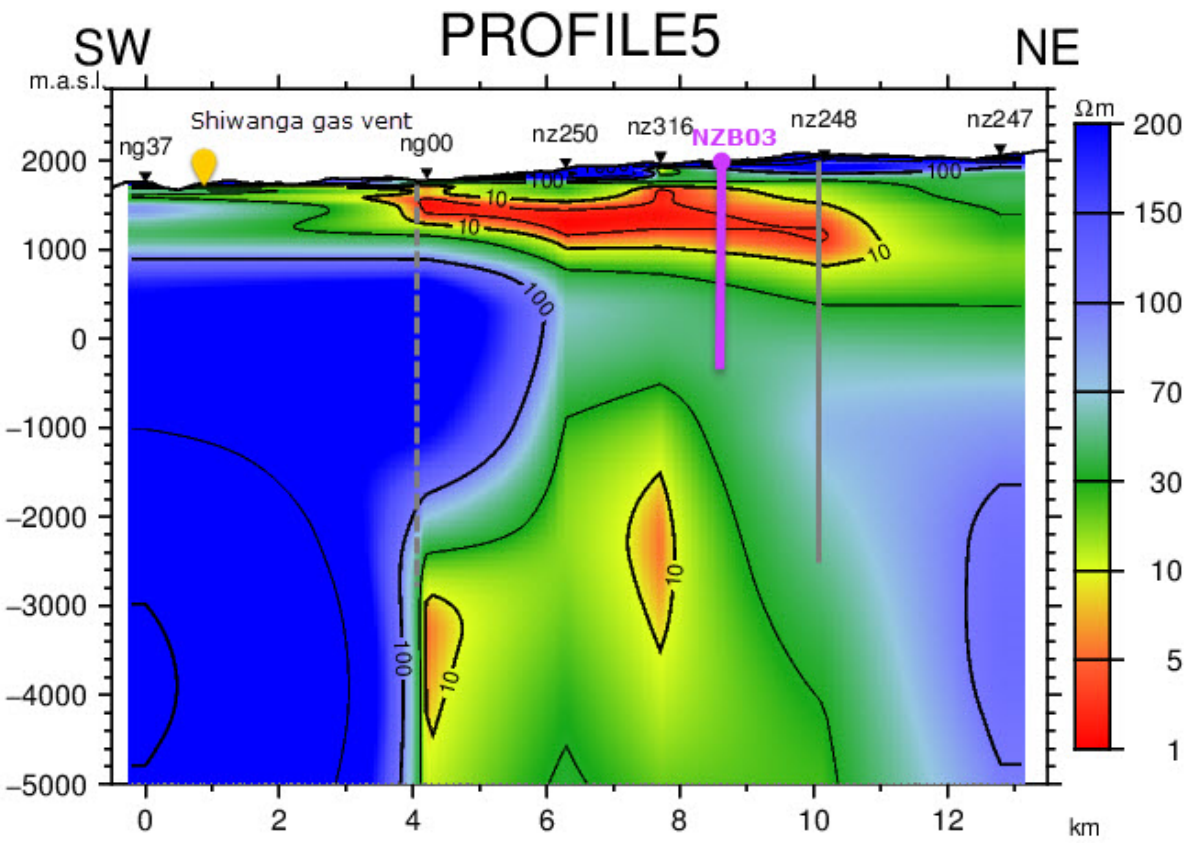

FIGURE 29: Proposed drilling target NZB03 (thick line);
the grey full and dashed lines are the mapped faults

11.1 Proposed drilling targets

The location of the proposed test drilling targets (shown in Figure 29) is based on the results of the integrated interpretation, including the geological, geochemical and resistivity results. The location of all proposed wells is shown in Figure 27. The three datasets have a good correlation as described in the previous section. The first three test drilling targets NZB01, NZB02 and NZB03 are located within the fault zone. Drilling site NZB01 is located about 1,800 m north of the Ngozi caldera to test the northern extension of the resource hosted in the fault zone (see Figure 27). NZB02 is located about 2 km west of the Ngozi caldera lake to investigate the west extension of the resource. Finally, NZB03 is located about 2,400 m south of the Ngozi caldera to test the southern extension of the geothermal reservoir observed in the MT soundings. All three proposed drilling sites are accessible by conventional drilling rigs as reported by TGDC ground truthing report (2017) (roads plotted in Figure 27). NZB01 is located at the same location as well NB-1 previously proposed by Norton Rose Fulbright and Omenda (2017). NZB03 is located about 2,000 m north of well NB-3 proposed by Alexander et al. (2016) and drilling site NZB02 is located about 2 km northeast of the NB-02 well proposed by Alexander et al. (2016), 3 km southwest of NB-5 proposed by Norton Rose Fulbright and Omenda (2017) and about 2.5 km southeast of the re-located NB-5 proposed by TGDC (2017). Drilling site NZB02 will need further ground truthing verification since it was not included in the survey by TGDC (2017).

12. ESTIMATED RESOURCE CAPACITY – VOLUMETRIC ASSESSMENT

An assessment of the geothermal resource in Ngozi has been made using a lognormal power density approach which provides most of the input parameters needed for a Monte Carlo stored heat assessment within a defined reservoir volume (i.e. heat stored in the rock matrix and heat stored in the reservoir fluid). This approach then estimates how much of that heat can reasonably be extracted and converted into power using typical technology (i.e. recovery factor). The lognormal power density approach for undrilled prospects like Ngozi first requires an estimate of the temperature of the reservoir based on geochemistry as well as porosity of the reservoir, extent, thickness, recovery factor, load factor, density of water, specific heat capacity of the reservoir rock and cut-off temperature (Wilmarth and Stimac, 2015; Cumming, 2016).

The resource area was estimated based on resistivity data as well as geological and geochemical results and interpretations. The reservoir was observed to be hosted in a fault zone, 7 km long and 4 km wide and thus covering an area of about 28 km^2. Estimates of selected input parameters are described below and summarized in Table 1.

- Resource areal extent is assessed 28 km^2, sealed within the fault zone (see Figure 27).
- Thickness of the reservoir ranges between 500 and 1,500 m based on the geological and geophysical results. We assume that the base of the clay cap is at 1,000 m a.s.l. as observed in resistivity cross-sections 5 and 9 located south and north of the Ngozi caldera, respectively.
- Based on geothermometry estimates, the average equilibrium temperature of the reservoir is 232±13°C. Hence, the maximum value, including the error range is 245°C, and the minimum value 219°C.
- Effective porosity lies between 3 and 8%, a typical effective porosity for fractured volcanic rocks, the older volcanic rocks on top of the basement in the Ngozi prospect.
- Cut-off temperature is 89°C, the temperature of the hot springs discharging below the Ngozi caldera lake.
- Recovery factor is between 5% (minimum) and 20% (maximum) with the best value being 12% of the stored heat in the reservoir.

TABLE 1: Estimates of selected input parameters for volumetric assessment of the heat stored in the Ngozi reservoir rock

Input variables	Units	Min.	Best value	Max.	Probability distribution
Area	km^2	2.9	N/A	28	Constant distribution
Thickness	m	500	1000	1500	Constant distribution
Rock density	kg/m^3	2700	2700	2700	Fixed value
Porosity	%	3	5	8	Triangular distribution
Recovery factor	%	5	12	20	Triangular distribution
Rock specific heat	J/kg °C	N/A	900	N/A	Fixed value
Temperature	°C	219	232	245	Triangular distribution
Fluid density	kg/m^3	N/A	864	N/A	Fixed value
Conversion efficiency	%	11.5	15.4	16.3	Triangular distribution
Fluid specific heat	J/kg °C	N/A	4510	N/A	Fixed value
Plant life	years	N/A	30	N/A	Fixed value
Load factor	%	N/A	95	N/A	Fixed value
Rejection temperature	°C	N/A	80	N/A	Fixed value

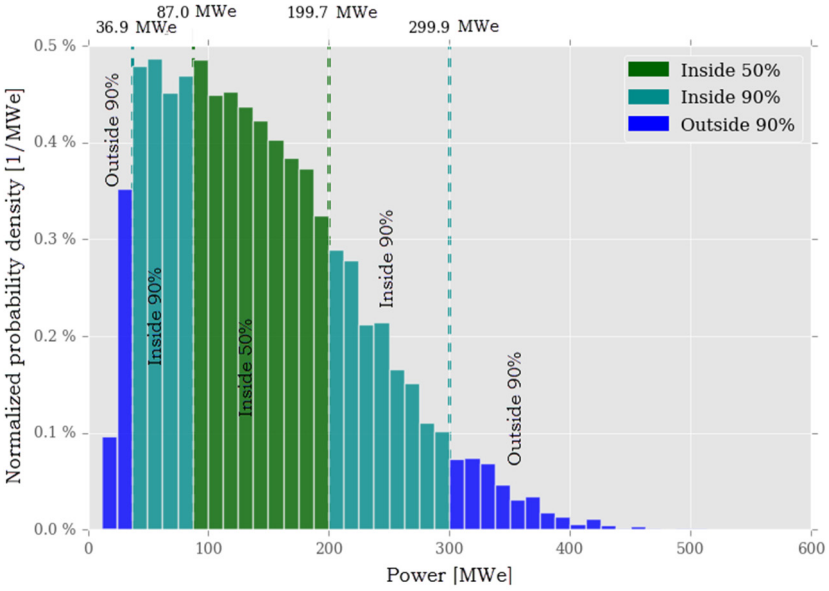

FIGURE 30: Probability distribution for electrical generation capacity for Ngozi geothermal field assuming 30 years of operation

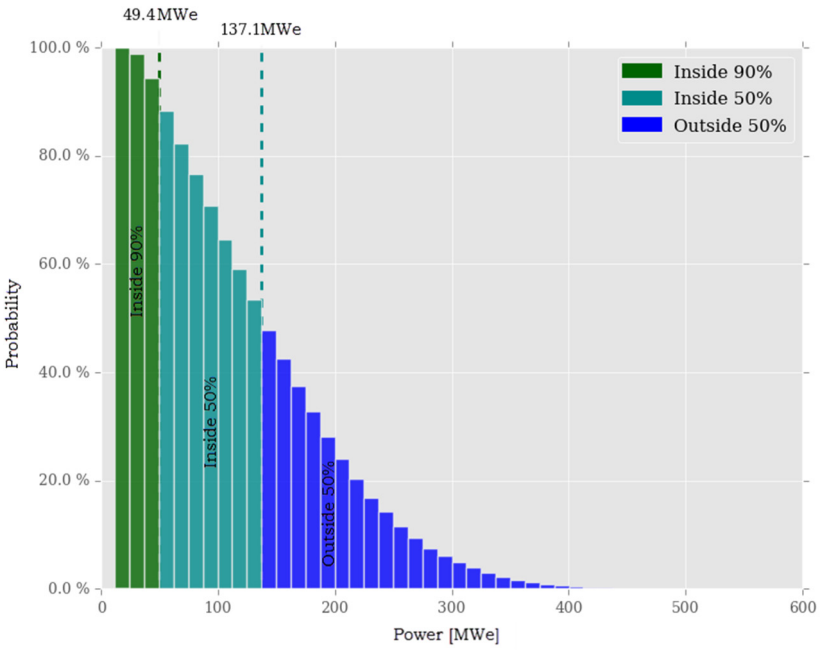

FIGURE 31: Cumulative probability distribution for electric generation capacity for Ngozi geothermal field assuming 30 years of operation

High (P90), Median (P50) and Low (P10) values for temperature and resource area are estimated. Finally, the power capacity distribution of the resource is computed from the product of the resource area and power density distributions all of which are assumed to be lognormal as indicated by the geothermal field population. The results of the volumetric assessment indicate that the electric generation capacity of Ngozi corresponds to **49 MWe** power generation for 30 years with a 90% confidence level.

The mean capacity for the same period is estimated at **137 MWe** (Figures 30 and 31). The 90% confidence range observed in the simulation result takes into account the uncertainties arising from insufficient knowledge about the reservoir conditions. As stated by Grant (2015) and Garg and Combs (2011), if the parameters for Monte Carlo calculations are overestimated, particularly the average resource thickness and recovery factor, this commonly results in inflated stored heat calculations. Hence, a careful evaluation of key parameters has to be done.

13. CONCLUSIONS

- Through the present study it has been possible to image the existence and define the extent of the geothermal resource of the Ngozi prospect. The resource is extensive and is hosted within a 4 km wide northwest trending fault zone which is about 7 km long and crosses Ngozi caldera.
- The Ngozi caldera lake is located within the fault zone, as well as the hot springs located at the bottom of the lake.

- Shallow intrusives observed within this fault zone at a depth of 3.5 to 4 km b.s.l. are believed to be heat sources of the geothermal system and seem to extend towards the Ngozi caldera.
- The smectite clay cap above the heat source is elevated and is likely to extend towards the Ngozi caldera. However, the absence of MT/TEM stations close to the Ngozi caldera does not allow this conclusion.
- Beyond 2,000 m northwest of the caldera there is limited indication for the extension of the geothermal resource. The only indication is the thick, extensive, very conductive layer which extends throughout the profiles, e.g. along profile 12. Such 500-1,000 m thick continuous layer could be associated with the clay rich sediments filling the depocentres, possibly with little interaction with geothermal activity. This observation indicates that the geothermal resource does not extend more than 2,000 m northwest of the Ngozi caldera.
- Unlike the previous studies, the current results are supported by both geological and geochemical results. The fault imaged from resistivity data was also mapped at the surface in a geological survey. This fault acts as a boundary to the geothermal resource to the west since the clay cap of the Ngozi caldera terminates along this fault.
- Similarly, the fault seems to connect the hot springs present below the Ngozi caldera, the only geochemical indicator for the existence of the high-temperature geothermal system and suggesting a reservoir temperature of 232°C estimated from Na-K geothermometers.
- Another important observational link is the Shiwaga CO_2 gas vent emitting significant amounts of predominantly magmatic CO_2 gas as well as its location within the resistivity anomaly. As resistivity observations indicate this vent is located in the peripheral part of the high-temperature geothermal system, it is likely that this part of the system is cooling down as it interacts with deep cold formations in the west. It is, however, also possible that the deep fault which brings this significant amount of CO_2 to the surface is not linked to the high-temperature geothermal system imaged in this study. Several studies have concluded that the origins of the CO_2 gases are deeper mantle sources including the one mined at Kiejo.
- Whether the alteration is in equilibrium with the temperature at present can only be verified by drilling. However, the geothermometry study using Na-K of the hot springs sampled at the bottom of the Ngozi caldera lake indicated a reservoir temperature of 232°C. This temperature is high enough for power generation in steam turbines.
- The lack of MT/TEM stations close to the Ngozi caldera masks a potentially important information. Stations here could help to constrain the geothermal system below the caldera where the only indication of a high-temperature geothermal system was found.

14. RECOMMENDATIONS

- Select a survey area, which consistently shows a geothermal system and do systematic MT/TEM infill.
- Perform 3D inversion of static shift corrected MT data in the selected areas as quality assurance to test the 1D imaging and to better define the resistivity anomalies. This applies especially to the deep conductive anomaly imaged in the 1D model which is interpreted as a heat source hosted within the extensive northwest trending fault zone.
- Perform 2D inversion with the purpose of imaging/modelling the conductive anomaly below the shallow conductive anomaly within the fault zone identified in this study.
- Systematic structural geological mapping of the area to reduce the uncertainties of the mapped faults. Most of the currently mapped faults are inferred or seen as lineaments from remote sensing data.
- MT/TEM survey infill close to stations nz316, nz315 and near the Ngozi caldera in order to confirm the extension of the updoming clay cap mapped at nz316 and fault zone which was observed to continue towards the Ngozi hot springs located at the bottom of the lake.

ACKNOWLEDGEMENTS

I would like to thank my employer Tanzania Geothermal Development Company Limited, TGDC, for allowing me to attend this six months training. It is difficult to find words to thank UNU-GTP in Iceland for the financial and technical support that enabled me to reach my goals. Thank you for covering all the costs for the six months training course in Iceland. I am greatly indebted to my supervisors, Gylfi Páll Hersir and Co-supervisors Knútur Árnason and Ásdís Benediktsdóttir. The integrated interpretation of the TEM and MT resistivity data, geology and geochemistry was not an easy task! Their close supervision, advice, guidance, endless discussions and constructive criticism are the lifeblood of my achievement. Our relationship was not strictly academic but you always treated me as a friend and I really value this! I am still impressed by the amount of references and books I was getting every time I asked a simple question. You created a positive atmosphere around me and made my life in Iceland enjoyable. Last but not least I want to thank my fellow UNU-GTP students. Thank you for helping me to face challenging times but also enjoying good times together during the whole period of my study.

REFERENCES

Alexander, B.K., Cumming, W., and Marini, L., 2016: *Geothermal resource assessment report. Ngozi and Songwe geothermal prospects, Tanzania. Final report – September 2016*. TGDC technical internal report, unpublished, 695 pp.

Anderson, E., Crosby, D. and Ussher, G., 2000: Bull's eye! – Simple resistivity imaging to reliably locate the geothermal reservoir. Proceedings of the World Geothermal Congress 2000, Kyushu-Tohoku, Japan, 909–914.

Archie, G.E., 1942: The electrical resistivity log as an aid in determining some reservoir characteristics. *Trans. AIME, 146, 54*-67.

Árnason, K., 2015: The static shift problem in MT soundings. *Proceedings of the World Geothermal Congress 2015, Melbourne, Australia,* 12 pp.

Árnason, K., 2006a: *TemX, short manual.* ÍSOR, Reykjavík, internal report, 17 pp.

Árnason, K., 2006b: TEMTD, *a program for 1D inversion of central-loop TEM and MT data*. ÍSOR – Iceland GeoSurvey, a short unpubl. manual, 17 pp.

Árnason K., 1989: *Central loop transient electromagnetic sounding over a horizontally layered earth*. Orkustofnun, Reykjavík, report OS-89032/JHD-06, 129 pp.

Árnason, K., Flóvenz, Ó., Georgsson, L.S., and Hersir, G.P., 1987: Resistivity structure of high-temperature geothermal systems in Iceland. *International Union of Geodesy and Geophysics (IUGG) XIX General Assembly*, *Vancouver Canada, Abstracts V*, 477.

Bahr, K., 1990: Geological noise in magnetotelluric data: a classification of distortion types. *Phys. Earth Planet. Inter., 66*, 24-38.

Bendat, J.S., and Piersol, A.G, 1971: *Random data: analysis and measurement procedures*. John Wiley, NY, 407 pp.

Berdichevsky, M.N., and Dmitriev, V.I., 2002: Magnetotellurics in the context of the theory of ill-posed problems. *Soc. of Expl. Geophys*. *11,* 137-138.

Calais, E., 2018: *The East African Rift.*
Website: *www.ics.purdue.edu/~ecalais/projects/ear/tectonics.jpg*

Chave, A.D., and Smith J.T., 1994: On electric and magnetic galvanic distortion tensor decompositions. *Geophys. Res*., *99,* 4669–4682.

Chave, D.A., Robe L.E., Ian, J.F, Alan, G.J., Randall, L.M., William, L.R., Ari, V., and Peter, W., 2012: *Introduction to the magnetotelluric method*. Cambridge University Press, 1-14.

Chi, M.A., and Browne, P.R.L., 1991: Alteration mineralogy of sediments in the Huka falls formation of the Te Mihi area, Wairakei. *Proceedings of the 13th New Zealand Geothermal Workshop, Auckland, NZ,* 185-191.

Cumming, W., 2009: A conceptual model approach to the geophysical exploration of permeable geothermal reservoirs that considers context and uncertainty. *79th Ann. Internat. Meeting, Soc. of Expl. Geophysicists, Expanded Abstracts*.

Cumming, W., 2016: Resource capacity estimates using log normal power density from producing fields and area from resource conceptual models: Advantages, pitfalls and remedies. *Proceedings of the 41st Workshop on Geothermal Reservoir Engineering, Stanford University, Stanford, CA*, 5 pp.

Cumming, W., and Mackie, R., 2010: Resistivity imaging of geothermal resources using 1D, 2D and 3D MT inversion and TDEM static shift correction illustrated by a Glass Mountain case history. *Proceedings of the World Geothermal Congress, Bali, Indonesia,* 10 pp.

Clarke, J., Gamble, T.D., Goubau, W.M., Koch, R.H., and Miracky, R.F., 1983: Remote reference magnetotellurics: Equipment and procedures. *Geophys. Prosp., 31*, 149-170.

Dakhnov, V.N., 1962: Geophysical well logging. *Colorado School of Mines, 57-2*, 445 pp.

Davatzes, N., and Hickman, S., 2009: Fractures, stress and fluid flow prior to stimulation of well 27-15, Desert Peak, Nevada, EGS Project. *Proceedings of the 34th Workshop on Geothermal Reservoir Engineering*, *Stanford University, Stanford, CA,* SGP-TR-187.

de Moor, J.M., Fischer, T.P., Sharp, Z.D., Hilton, D.R., Barry, P.H., Mangasini, F., and Ramirez C., 2012: Gas chemistry and nitrogen isotope compositions of cold mantle gases from Rungwe volcanic province, southern Tanzania. *Chemical Geology, 339,* 30-42.

DECON, SWECO and Inter-Consult 2005: *Tanzania rural electrification study and technical report on geothermal power*. Activity 1.4.1, Dar es Salaam, Tanzania, 22 pp.

Delalande, M.M., Gherardi, F., Williamson, D., Kajula, S., Kraml, M., Noret, A., Abdallah, I., Mwandapile, E., Massault, M., Majule, A., and Bergonzini, L., 2015: Hydrogeochemical features of Lake Ngozi (SW Tanzania). *African earth Sciences, 103*, 153-167.

Delvaux, D. and Hanon, M., 1993: Neotectonics of the Mbeya area, SW Tanzania. *Mus. Roy. Afr. Centr., Tervuren (Belg.), Dépt. Géol. Min., Rapp. ann. 1991-1992,* 87-97.

Delvaux, D., Kervyn, R., Vittori, E., Kajara, R.S.A., and Kilembe, E., 1998: Late Quaternary tectonic activity and lake level fluctuation in the Rukwa rift basin, East Africa. *African earth Sciences*, *26*, 397-421.

Delvaux, D., Kraml, M., Sierralta, M., Wittenberg, A., Mayalla, J.W., Kabaka, K., Makene, C., and Geothermal working group, 2010: Surface exploration of a viable geothermal resource in Mbeya area, SW Tanzania. Part I: Geology of the Ngozi-Songwe geothermal system. *Proceedings of the World Geothermal Congress 2010, Bali, Indonesia*, 7 pp.

Delvaux, D., Levi, K., Kajara, R. and Sarota, J., 1992: Cenozoic paleostress and kinematic evolution of the Rukwa - North Malawi rift valley (East African rift system). *Bulletin des Centres de Recherches Exploration Production Elfaquitaine, 16,* 383-406.

Didas, M.M., 2018: Appendices to the report: *"1D joint inversion of MT and TEM data from Ngozi geothermal prospect, SW-Tanzania. An integrated interpretation of geoscientific results".* UNU-GTP, Iceland, report 13 appendices, 97 pp.

Ebinger, C.J., Deino, A.L., Drake, R.E., and Thesa, A.L., 1989: Chronology of volcanism and rift basin propagation: Rungwe volcanic provinces, East Africa. *J. Geophysical Research*, *94,* 15.783-15.803.

Ebinger, C.J., Deino A.L., Tesha A.L., Becker, T., and Ring, U., 1993: Regional tectonic controls on rift basin morphology: evolution of the Northern Malawi (Nyasa) Rift. *J. Geophysical Research, 98,* 17.821-17.836.

ELC and TGDC, 2017: *Surface exploration and training in Kiejo-Mbaka geothermal area, Tanzania*. ELC-Electroconsult S.P.A., and Tanzania Geothermal Development Company, Ltd. – TGDC, unpubl. report, 98 pp.

Eysteinsson, H., 1998: *TEMMAP and TEMCROSS plotting programs*. ÍSOR – Iceland GeoSurvey, Reykjavík, unpublished programs and manuals.

Flóvenz, Ó., Hersir, G., Saemundsson, K., Ármannsson, H., and Fridriksson, T., 2012: Geothermal energy exploration techniques. In: Sayigh, A, (ed.): Comprehensive renewable energy, 7. Elsevier, Oxford, 51-95.

Flóvenz, Ó.G., Spangerberg, E., Kulenkampff, J., Árnason, K., and Karlsdóttir, R., and Huenges, E., 2005: The role of electrical interface conduction in geothermal exploration. *Proceedings of the World Geothermal Congress 2005, Antalya, Turkey,* 9 pp.

Fontijn, K., Delvaux, D., Ernst, G.G.J., Kervyn, M., Mbede, E., and Jacobs, P., 2010a: Tectonic control over active volcanism at a range of scales: Case of the Rungwe volcanic province, SW Tanzania; and hazard implications. *J. African earth Sciences, 58*, 764-777.

Fontijn, K., Ernst, G.G.J., Elburg, M.A., Williamson, D., Abdallah, E., Kwelwa, S., Mbede, E., and Jacobs, P., 2010b: Holocene explosive eruption in the Rungwe volcanic province, Tanzania. *J. Volc. Geoth. Res., 196,* 91-110

Fontijn, K., Williamson, D., Mbede, E. and Ernst, G.G.J., 2012: The Rungwe volcanic province, Tanzania – a review. *J. African earth Sciences, 63*, 12-31.

Gamble, T.D., Goubau, W.M., and Clarke, J., 1979: Magnetotellurics with a remote magnetic reference. *Geophysics*, *44*, 53-68.

Garg, S., and Combs, J., 2011: A reexamination of USGS volumetric "heat in place" method. *Proceedings of the 36th Workshop on Geothermal Reservoir Engineering*, *Stanford University, Stanford, CA,* 5 pp.

Grant, M., 2015: Resource assessment, a review, with reference to the Australian Code. *Proceedings of the World Geothermal Congress 2015*, *Melbourne, Australia,* 6 pp.

Gibert, E., Bergonzini, L., Massault, M. and Williamson, D., 2002: AMS-14 C chronology of 40.0 cal ka BP continuous deposits from a crater lake (Lake Masoko, Tanzania). *Palaeogeography, Palaeoclimatology, Palaeoecology 187,* 307-322.

Hersir, G.P., and Árnason, K., 2009: Resistivity of rocks. *Paper presented at Short Course on Surface Exploration for Geothermal Resources, Ahuachapan and Santa Tecla, El Salvador, UNU-GTP, Iceland and LaGeo,* 8 pp.

Hersir, G.P., Árnason, K., and Vilhjálmsson, A.M., 2015b: 3D inversion of magnetotelluric (MT) data from Krýsuvík, high temperature geothermal area in SW Iceland. *World Geothermal Congress 2015 Melbourne, Australia*, 14 pp.

Hersir, G.P., Kristinsson, G.S., and Mnjokava, T.T., 2015a: *Tanzania visit in January 2015; assessment of areas for surface exploration studies and training needs*. TGDC and ISOR, technical report, 48 pp.

Hochstein, M.P., Temu, E.B and Moshy, C.M.A., 2000: Geothermal resources of Tanzania. *Proceedings of the World Geothermal Congress 2000*, *Kyushu-Tohoku, Japan*, 1233-1238.

Ingham, M.R., and Hutton, V.R.S., 1982: Crustal and upper mantle electrical structure in southern Scotland. *Geophysics, 69*, 579-594.

JICA, 2014: *Data collection survey on geothermal energy development in East Africa*. JICA, Japan, final report (Tanzania), 109 pp.

Jones, A.G., 1983: The problem of current channelling, a critical review. *Surveys in Geophysics*, *6-1*, 79-122.

Jones, A.G, 2008: *Magnetotellurics for natural resources: From acquisition through interpretation*. Dublin Institute for Advanced Studies (DIAS), Dublin, 17–18.

Jones, A.G., and Groom, R.W., 1993: Strike-angle determination from the magnetotelluric impedance tensor in the presence of noise and local distortion: rotate at your peril. *Geophysical J. International*, *113-2*, 524-534.

Josephat, S., 2016: Geothermometry and quantifying of mixing and water-rock interactions in the Ngozi geothermal field, SW-Tanzania. Report 26 in: *Geothermal training in Iceland 2016*. UNU-GTP, Iceland. 289-310.

Kalberkamp, U., Schaumann, G., Ndonde, P.B., Chiragwile, S.A., Mwano, J.M and GEOTHERM Working Group, 2010: Surface exploration of a viable geothermal resource in Mbeya area, SW Tanzania. Part III: Geophysics. *Proceedings of the World Geothermal Congress 2010, Bali, Indonesia,* 6 pp.

Keller, G.V., and Frischknecht, F.C., 1966: *Electrical methods in geophysical prospecting.* Pergamon Press Ltd., Oxford, 527 pp.

Kraml, M., Schaumann, G., Kalberkamp, U., Stadtler, C., Delvaux, D., Ndonde, P.B., Mnjokava, T.T., Chiragwile, S.A., Mayalla, J.W., Kabaka, K., Mwano, J.M., and Makene, C., 2008: *Geothermal energy as an alternative source of energy for Tanzania.* BGR, Germany, GEOTHERM project, Technical cooperation with the Republic of Tanzania, final technical report, 235 pp.

Kristinsdóttir, L.H., Flóvenz, Ó.G., and Árnason K., 2010: Electrical conductivity and P-wave velocity in rock samples from high-temperature Icelandic geothermal fields. *Geothermics, 39*, 94-105.

Kristmannsdóttir, H., 1979: Alteration of basaltic rocks by hydrothermal activity at 100-300°C. In: Mortland, M.M., and Farmer, V.C. (editors), *International Clay Conference 1978*. Elsevier Scientific Publishing Co., Amsterdam, 359-367.

Marobhe, I.M., 1989: *Interpretation of aerogeophysical anomalies of Southwestern Tanzania.* Geological Survey of Finland, Bulletin 350, PhD thesis, 78 pp.

McNitt, J.R., 1982: *The geothermal potential of East Africa*. UNESCO/USAID Geothermal Seminar, Nairobi, Kenya, June, 1–9.

Mnjokava, T.T., 2014: Geothermal development in Tanzania - Status report. *Paper presented at Short Course IX on Exploration for Geothermal Resources, organized by UNUGTP, GDC and KenGen, at Lake Bogoria and Lake Naivasha, Kenya*, 8 pp.

Norton Rose Fulbright and Omenda P., 2017: *Consultancy services for preparation of geothermal energy development projects proposal document and M&E system manual for the project. Project proposal document for geothermal resource development*. TGDC – technical internal report, unpubl. 139 pp.

Ochmann, N., and Garofalo, K., 2013: *Geothermal energy as an alternative source of energy for Tanzania.* GEOTHERM - Project 2002.2061.6, final technical report of phase II (2010-2013), technical cooperation with United Republic of Tanzania*,* unpubl. report, 156 pp.

Openei, 2018: *OpenEI*. Website: *en.openei.org/wiki/Magnetotellurics.*

Park, S.K., and Livelybrook, D.W., 1989: Quantitative interpretation of rotationally invariant parameters in Magnetotellurics. *Geophysics, 54,* 1484-1490.

Parkinson, W., 1959: Directions of rapid geomagnetic fluctuations. G*eophys. J. Internat., 2-1*, 1-14.

Pellerin, L., and Hohmann, G.W., 1990: Transient electromagnetic inversion: A remedy for magnetotelluric static shifts. *Geophysics, 55-9,* 1242-1250.

Phoenix, 2005: *Data processing user guide, SSMT2000, NPIPlot, MTEditor, synchro time series View*. Phoenix Geophysics, Ltd., Toronto, Canada

Phoenix, 2018: *Phoenix Geophysics*, website: *www.phoenix-geophysics.com/home.*

Pinna, P., France, Bureau de recherches géologiques et minières, Chuo Kikuu cha Dar es Salaam, Geological Survey of Tanzania, BRGM and 20th Colloquium on African Geology, 2008: *Geology and mineral map of Tanzania*. Orléans, France.

Quist, A.S., and Marshall W.L., 1968: Electrical conductances of aqueous sodium chloride solutions from 0 to 800°C and at pressures to 4000 bars. *J. Physical Chemistry, 72,* 684-703.

Ranganayaki, R.P., 1984: An interpretive analysis of magnetotelluric data. *Geophysics*, *49,* 1730-1748.

Schmucker, U., 1970: Anomalies of geomagnetic variations in the southwestern United States. *University of California Press, Bull. Scripps Inst. Oceanography. 13,* 175 pp.

SOHO, 2010: *Solar wind.* Solar and Heliospheric Observatory,
website: *sohowww.nascom.nasa.gov/gallery/images/magfield.html.*

Sternberg, B.K., Washburne J.C., and Pellerin, L., 1988: Correlation for the static shift in magnetotellurics using transient electromagnetic soundings. *Geophysics, 53,* 1459-1468.

SWECO, 1978: *Reconnaissance of geothermal resources*. SWECO, Stochholm, report for the Ministry of Water, Energy and Minerals of Tanzania, 51 pp.

TGDC, 2017: *Ground truthing survey of the new proposed slim holes locations in Ngozi geothermal prospect.* Tanzania Geothermal Development Company, Ltd., internal technical report, unpubl. 16 pp.

TGDC, 2018: *Geothermal development in Tanzania.* TGDC, presentation to stakeholders, Dodoma, 13 pp.

Ussher, G., Harvey, C., Johnstone, R., and Anderson E., 2000: Understanding resistivities observed in geothermal systems. *Proceedings of the World Geothermal Congress 2000, Kyushu-Tohoku, Japan,* 1915-1920.

Vozoff, K., 1991: The magnetotelluric method. In: Nabighian, M.N. (ed.), *Electromagnetic methods in Applied geophysics, 2B*. SEG, Tulsa, OK, 641–711.

Walker, B.G., 1969: Springs of deep seated origin in Tanzania. *Proceedings of the 23rd Intern. Geological Congress,* 19.

Ward, S.H., and Wannamaker, P.E., 1983: *The MT/AMT electromagnetic method in geothermal exploration*. UNU-GTP, Iceland, report 5, 107 pp.

Wight, D.E., and Bostick, F.X., 1980: Cascade decimation – A technique for real time estimation of power spectrum. *Proceedings of IEEE Intern Conf. Acoustic, Speech signal processing, Soc. Explor. Geophys.,* 626-629.

Wight, D.E.; Bostick, F.X., and Simth, H.W., 1977: *Real time Fourier transformation of Magnetotelluric data.* University of Texas, Austin, Tech. report, EGRL/EERL.

Wilmarth, M., and Stimac, J., 2015: Power density in geothermal fields. *Proceedings of the World Geothermal Congress, Melbourne, Australia*, 7 pp.

Zonge, 2018: *Zonge International*. Zonge,
website: www.zonge.com/geophysical-methods/electrical-em/tem/